DOI: 10.1002/chem.200902026

A Simple Chemical Tuning of the Effective Concentration: Selection of Single-, Double-, and Triple-Stranded Binuclear Lanthanide Helicates

Emmanuel Terazzi,* Laure Guénée, Bernard Bocquet, Jean-François Lemonnier, Natalia Dalla Favera, and Claude Piguet*[a]

Dedicated to Professor Jean-Claude G. Bünzli on the occasion of his 65th birthday

Abstract: The replacement of terminal 2-benzimidazol-6-carboxypyridine (two internal rotational degrees of freedom) with 2-benzimidazol-8-hydroxyquinoline (one internal rotational degree of freedom) into segmental bis-tridentate ligands in going from **L2** and [**L3**-2H]$^{2-}$ to [**L12b**-2H]$^{2-}$ does not significantly affect the structures of the resulting binuclear lanthanide triple-stranded helical complexes $[Ln_2(\mathbf{L2})_3]^{6+}$, $[Ln_2(\mathbf{L3}\text{-}2H)_3]$, and $[Ln_2(\mathbf{L12b}\text{-}2H)_3]$ (palindromic helices, intermetallic contact distance $\approx$9 Å, helical pitch $\approx$1.4 nm per turn). However, their thermodynamic assemblies are completely different in solution, as evidenced by the spectacular decrease of the effective concentrations by two orders of magnitude for [**L12b**-2H]$^{2-}$. This key parameter in the $[Ln_2(\mathbf{L12b}\text{-}2H)_n]$ (n=2, 3) complexes is further abruptly modulated along the lanthanide series (Ln=La to Lu), which provides an unprecedented tool for 1) tuning the number of ligand strands in the final helicates, 2) selectively coordinating lanthanides in the various complexes, and 3) controlling the ratio of lanthanide-containing polymers over discrete assemblies.

Keywords: effective concentration · helical structures · lanthanides · self-assembly · thermodynamics

Introduction

The assembly of the first binuclear lanthanide triple-stranded helicates $[Ln_2(\mathbf{L1})_3]^{6+}$ (Ln^{III} is a trivalent lanthanide) were reported more than fifteen years ago. It relied on the well-established concept of a judicious matching between the binding possibilities of the ligands (segmental bis-tridentate and helical twist) and the stereochemical preferences of the metals (nine-coordinate, no ligand field).[1] The subsequent systematic exploitation of this approach with the related segmental ligands **L2**–**L5**—in which 1) the nature of the donor atoms of the tridentate binding sites were somehow varied, but 2) the two degrees of freedom produced by internal rotations about the central pyridine ring were retained—produced binuclear $[Ln_2(\mathbf{L}k)_3]^{6+}$ (k=1, 2),[1,2] $[Ln_2(\mathbf{L3}\text{-}2H)_3]$,[3] trinuclear $[Ln_3(\mathbf{L4})_3]^{9+}$,[4] and tetranuclear $[Ln_4(\mathbf{L5})_3]^{12+}$[5] triple-stranded helicates (Scheme 1). The metal-centered luminescence of these helicates and that of the closely related system $[Ln_2(\mathbf{L6}\text{-}2H)_3]$[6] gave some valuable insights into the intimate mechanisms of intramolecular f–f energy-transfer processes.[1–6] The recent decoration of ligand **L3** with water-solubilizing groups opened remarkable perspectives for the use of some derivatives of $[Ln_2(\mathbf{L3}\text{-}2H)_3]$ as bioprobes.[7] Because of the transparency of biological tissue toward near-infrared (NIR) radiation, the field of lanthanide bioprobes evolved toward the design of novel ligands, which were able 1) to accommodate an efficient NIR emitter (Ln=Pr, Nd, Er, Yb), and 2) to extend the potential excitation light sources into the visible part of the electromagnetic spectrum.[8] In this context, considerable efforts have been focused on the incorporation of the fused heterocyclic bidentate 8-hydroxyquinoline unit into tridentate binding ligands **L7**–**L10**, in which an additional donor group is connected at the 2-position of the pyridine ring (Scheme 2).[9–12] Upon deprotonation of the phenol ring and

[a] Dr. E. Terazzi, Dr. L. Guénée, B. Bocquet, Dr. J.-F. Lemonnier, N. Dalla Favera, Prof. Dr. C. Piguet
Department of Inorganic, Analytical and Applied Chemistry
University of Geneva, 30 quai E. Ansermet
1211 Geneva 4 (Switzerland)
Fax: (+41) 22-379-6830
E-mail: Emmanuel.Terazzi@unige.ch
Claude.Piguet@unige.ch

Supporting information for this article is available on the WWW under http://dx.doi.org/10.1002/chem.200902026. This includes the synthesis of ligand **L10b** and statistical factors for complexes used in multilinear least-squares fits; tables of crystallographic data and geometrical analyses; tables of elemental analyses; ESIMS titrations and thermodynamic data; schemes and figures showing the synthetic, spectroscopic, crystallographic, and thermodynamic data; and cif files for the crystal structures of **7** and **10**.

complexation with trivalent lanthanides, the saturated neutral $[Ln(\mathbf{L}k\text{-}H)_3]$ complexes ($k=7$–10) are readily formed as mixtures of head-to-head-to-head (*HHH*, C_3-symmetrical) and head-to-head-to-tail (*HHT*, C_1-symmetrical) isomers. A ligand-centered charge-transfer band develops in the visible domain, which can be exploited for sensitizing NIR lanthanide emitters.[10–12]

Though the isolation of a single isomer may result from lucky crystallization processes, or through selective interactions of the coordinated phenolate anions with cocrystallized alkaline cations,[10–12] more reliable strategies are to 1) connect three parallel tridentate binding units to a covalent tripod,[9,10] or 2) link two opposite tridentate binding units to a symmetrical spacer as found in ligands **L11** and **L12**. The latter approach leads to the formation of two identical *HHH* nine-coordinated building blocks related by two-fold symmetry axes in the final binuclear helicates $[Ln_2(\mathbf{L11}\text{-}2H)_3]$ (Ln = Eu, Yb)[13] and $[Ln_2(\mathbf{L12a}\text{-}2H)_3]$ (Ln = La, Nd).[12]

The existence of neutral D_3-symmetrical triple helices for $[Ln_2(\mathbf{L11}\text{-}2H)_3]$ has been established both in the solid state (Yb···Yb = 7.77 Å) and in solution. The stability constants in anhydrous acetonitrile [equilibrium shown in Eq. (1); $\log(\beta_{2,3}^{Eu,L11\text{-}2H}) = 26.1(3)$ and $\log(\beta_{2,3}^{Yb,L11\text{-}2H}) = 25.7(3)$],[13] although similar to those found for the charged helicates $[Ln_2(\mathbf{L}k)_3]^{6+}$ ($k=1$, 2),[1,2] are alarmingly low and can be compared with $\log(\beta_{2,3}^{Eu,L3\text{-}2H}) \approx 51$ ($9.8 < pH < 10.4$)[3] estimated for $[\mathbf{L3}\text{-}2H]^{2-}$ in water, a solvent as competitive as acetonitrile for complexation with trivalent lanthanides.[3,7]

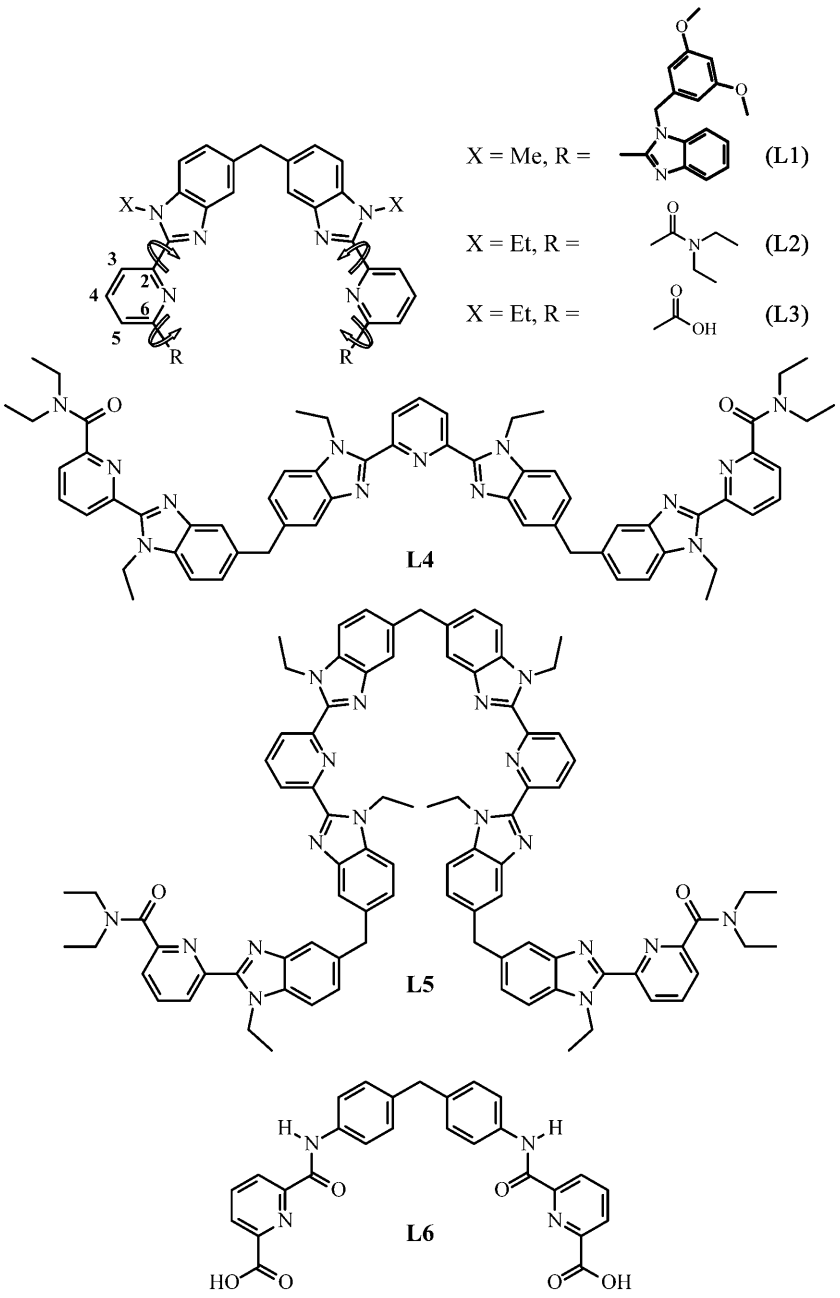

Scheme 1. Chemical structures with numbering scheme for the central pyridine rings of the segmental multitridentate ligands **L1**–**L6**. The curved arrows highlight the free rotations about the single bonds connected to the central pyridine rings.

$$3\,[\mathbf{L11}\text{-}2H]^{2-} + 2\,[Ln(CH_3CN)_9]^{3+} \rightleftharpoons [Ln_2(\mathbf{L11}\text{-}2H)_3] + 18\,CH_3CN \quad (1)$$

$\beta_{2,3}^{Ln,L11\text{-}2H}$

According to the concept that any metal–ligand assembly [equilibrium shown in Eq. (2)] can be modeled with the help of five microscopic thermodynamic parameters in Equation (3), we suspect that a thorough understanding of the thermodynamic process leading to $[Ln_2(\mathbf{L2})_3]^{6+}$, $[Ln_2(\mathbf{L3}\text{-}2H)_3]$, and $[Ln_2(\mathbf{L12}\text{-}2H)_3]$ may deliver some clues for programming selectivity and stability along the lanthanide series ($\omega_{m,n}^{M,L}$ is the statistical factor of the assembly,[14] $f_{inter}^{M,L}$ is the absolute intermolecular affinity (including desolvation) of one site of the ligand for the entering metal, c^{eff} is the effective concentration used to estimate the preorganization

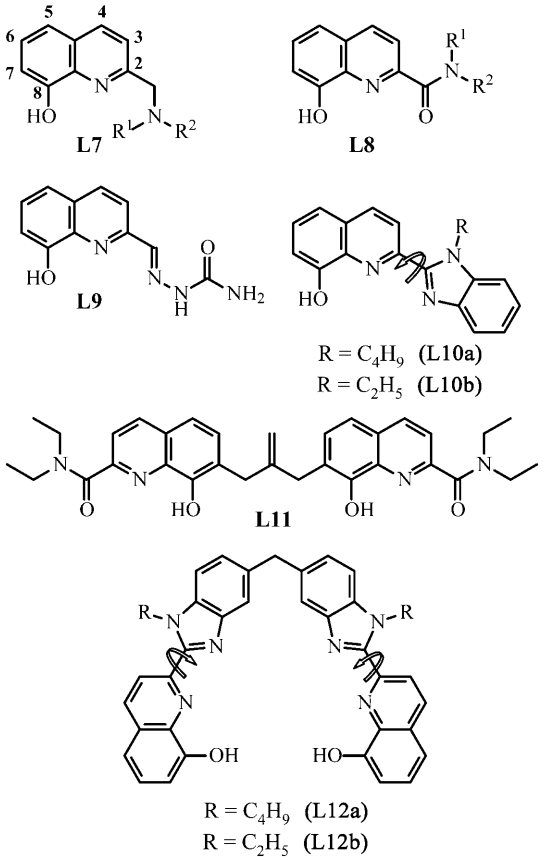

Scheme 2. Chemical structures of the ligands **L7**–**L12** incorporating 8-hydroxyquinoline units with the numbering scheme. The curved arrows highlight the free rotations about the single bonds connecting the benzimidazole and the quinoline rings.

of the receptor for intramolecular macrocyclization reactions ($f_{\mathrm{intra}}^{\mathrm{M,L}}=c^{\mathrm{eff}}f_{\mathrm{inter}}^{\mathrm{M,L}}$), and $u_i^{\mathrm{M,M}}=e^{-\Delta E_i^{\mathrm{MM}}/\mathrm{RT}}$ and $u_j^{\mathrm{L,L}}=e^{-\Delta E_j^{\mathrm{LL}}/\mathrm{RT}}$ are the Boltzmann factors measuring intermetallic and interligand interactions in the final helicate, respectively).[15]

$$m\,\mathrm{M}^{z+}+n\,\mathrm{L}\rightleftharpoons[\mathrm{M}_m\mathrm{L}_n]^{mz+}\quad \Delta G_{m,n}^{0\mathrm{M,L}}=-RT\ln(\beta_{m,n}^{\mathrm{M,L}}) \tag{2}$$

$$\begin{aligned}\beta_{m,n}^{\mathrm{M,L}}&=\omega_{m,n}^{\mathrm{M,L}}(f_{\mathrm{inter}}^{\mathrm{M,L}})^{mn}(c^{\mathrm{eff}})^{mn-n-m+1}\prod_i e^{-\Delta E_i^{\mathrm{M,M}}/RT}\prod_j e^{-\Delta E_j^{\mathrm{L,L}}/RT}\\&=\omega_{m,n}^{\mathrm{M,L}}(f_{\mathrm{inter}}^{\mathrm{M,L}})^{mn}(c^{\mathrm{eff}})^{mn-n-m+1}\prod_i u_i^{\mathrm{M,M}}\prod_j u_j^{\mathrm{L,L}}\end{aligned} \tag{3}$$

Among the different candidates for rationalizing the drastic decrease in stability by twenty-five orders of magnitude in going from $[Ln_2(\mathbf{L3}\text{-}2H)_3]$ (water) to $[Ln_2(\mathbf{L11}\text{-}2H)_3]$ (acetonitrile), the lower polarity of acetonitrile is a crucial point, as it reduces the entropy gain produced by the charge neutralization accompanying the complexation processes.[16] However, some variations of the effective concentration, c^{eff}, which measures the degree of preorganization of the receptor for the specific intramolecular macrocyclization processes operating in the formation of triple-stranded helicates, may also significantly contribute to their final stabilities. In this context, the reduction of the number of rotational degrees of freedom per tridentate binding unit in going from **L1**–**L6** ($n=2$, see curved arrows in Scheme 1) to **L7**–**L12** ($n=1$, see curved arrows in Scheme 2) is appealing, and ligand **L12** is ideally suited for elucidating the effect produced by the fusion of the terminal phenol ring with the central pyridine ring in the 8-hydroxyquinoline moieties because the diphenylmethane spacers are identical in **L1**–**L5** and **L12**.[17–19] Moreover, a preliminary NMR spectroscopy report by Bünzli and co-workers on the formation of $[La_2(\mathbf{L12a}\text{-}2H)_3]$ confirmed the formation of the binuclear triple helix in solution, but solubility problems and complicated behaviors along the lanthanide series prevented further characterizations except for the recording of photophysical data in $[Nd_2(\mathbf{L12a}\text{-}2H)_3]$.[12] These two points are encouraging for the investigation of unprecedented thermodynamic changes along the series. In this contribution, we thus focus on the exploration of the formation of the binuclear triple-stranded helicates $[Ln_2(\mathbf{L12b}\text{-}2H)_3]$, with the two following specifications in mind: 1) an analysis of the molecular structure of $[Ln_2(\mathbf{L12b}\text{-}2H)_3]$, followed by its comparison with $[Ln_2(\mathbf{L2})_3]^{6+}$ and $[Ln_2(\mathbf{L3}\text{-}2H)_3]$, and 2) a thermodynamic analysis of the formation of $[Ln_2(\mathbf{L12b}\text{-}2H)_3]$ and $[Ln_2(\mathbf{L2})_3]^{6+}$ along the lanthanide series.

Results and Discussion

Synthesis of the ligands: The segmental ligand **L12b** is obtained in a good global yield (48%) by means of a convergent six-step synthetic procedure (Scheme 3). An improved preparation of the precursor **3**[20] starts with the O-benzyl protection of 8-hydroxyquinaldine to give **1**. A subsequent two-step oxidation using SeO_2 followed by treatment with $H_2NSO_3H/NaClO_2$ provides, successively, the aldehyde **2** and the carboxylic acid **3**. The benzyl-protected ligand **7** is then obtained by condensation between precursors **3** and **5**,[21] followed by a double-reductive modified Philips coupling reaction.[22] Finally, **7** is deprotected by reaction with BBr_3 and yields the bis-tridentate ligand **L12b**. Its ^{1}H NMR spectrum confirms the existence of a dynamically averaged C_{2v} symmetry on the NMR spectroscopic timescale (eight signals for the aromatic protons, two pairs of enantiotopic methylene protons in 1:2 ratio, and two signals for methyl groups) as previously reported for the analogous ligand **L12a**.[12] The parent monotopic tridentate ligand **L10b** (Scheme 2) is prepared by using the same synthetic strategy in three steps from **3** and **4**[21] (yield 42%; see Scheme S1 in the Supporting Information).

For the two uncomplexed ligands **L10b** and **L12b**, the lack of a nuclear Overhauser enhancement (NOE) effect between the ethyl residues of the benzimidazole ring and the protons connected at the 3-position of the quinoline ring (see Scheme 2 for numbering) agrees with a *trans* arrangement of the N-donor atoms borne by the adjacent aromatic rings (Scheme 3). Slow evaporation of a solution of the precursor ligand **7** in CH_2Cl_2/MeOH gives colorless prisms, for

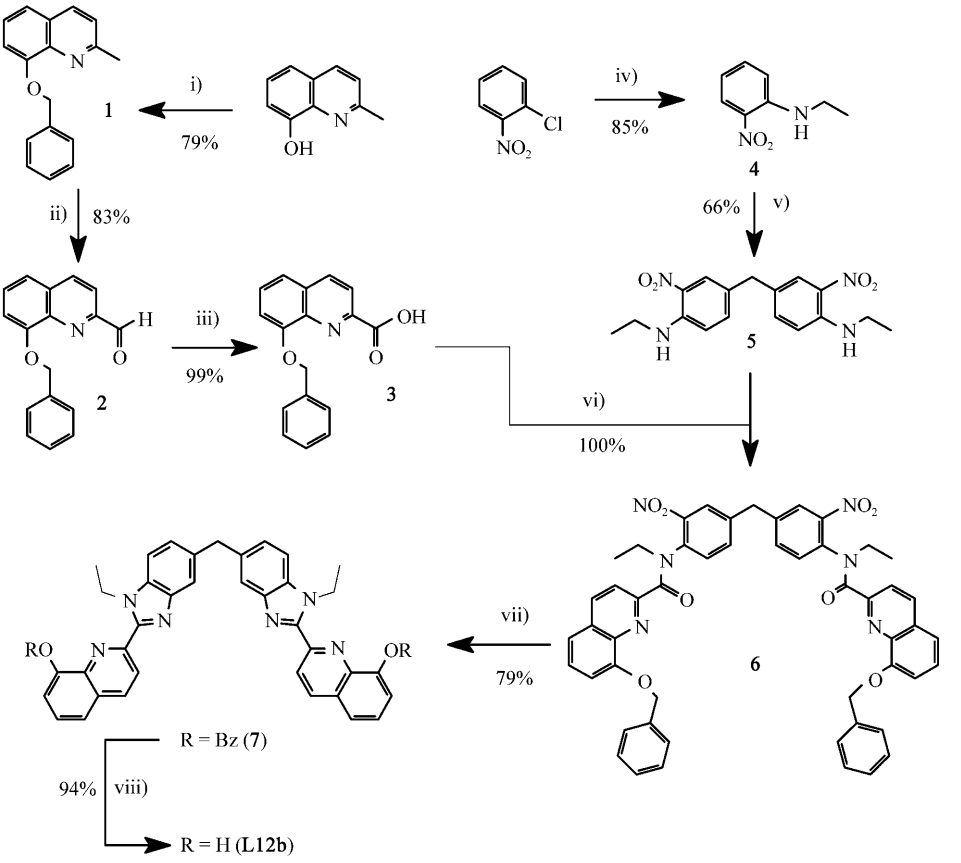

Scheme 3. Reagents: i) benzyl bromide, K_2CO_3, KI (cat.), acetone; ii) SeO_2, dioxane; iii) H_2NSO_3H, $NaClO_2$, H_2O/THF; iv) $EtNH_2$/DMSO; v) $(CH_2O)_n$/HCl (37%); vi) compound **3**, $SOCl_2$, DMF (cat.), CH_2Cl_2, then **5**, CH_2Cl_2, diisopropylethylamine; vii) Fe, H_2O/EtOH, HCl (37%); viii) BBr_3 (1 M) in CH_2Cl_2.

which the X-ray crystal structure, shown in Figure 1, confirms that the tridentate binding units adopt the expected *trans* conformation, which minimizes the global dipole momentum (i.e., the coordinating N-benzimidazole atom is *trans* to the N-quinoline atom with respect to the interannular C–C bond). Because of the fused character of the hydroxyquinoline ring, the O-benzyl-protected quinoline atom is forced to adopt a constrained *cis* planar conformation with the adjacent N-quinoline atom, which contrasts with the more flexible *trans–trans* arrangement found for tridentate 2,6-disubstituted pyridine units in ligands **L1**–**L6**.[2–5] Bond lengths and bond angles are standard (Tables S1–S3 in the Supporting Information),[23] and the ligand possesses a pseudo-twofold axis along the c direction and passing through C26. Two intermolecular stacking interactions can be detected in the unit cell (Figure S1 and Table S3 in the Supporting Information).

Finally, the quantitative analysis of the helicity of the diphenylmethane spacer, defined as a five-atom crooked line (C19-C20-C26-C46-C45 in **7**), by using Equation (4)[24] gives a helicity index (H) of 0.13, which is diagnostic for a negligible helical preorganization of the ligand strand (L = 3.51 Å is the end-to-end distance of the helix taken as the C19···C45 contact distance; A = 0.215 Å^2 is the area of the subtended figure produced by the projection of the five atoms onto a plane perpendicular to the helical axis defined by the line passing through two terminal atoms of the chain; and D = 5.82 Å is the total length of the crooked line).[25]

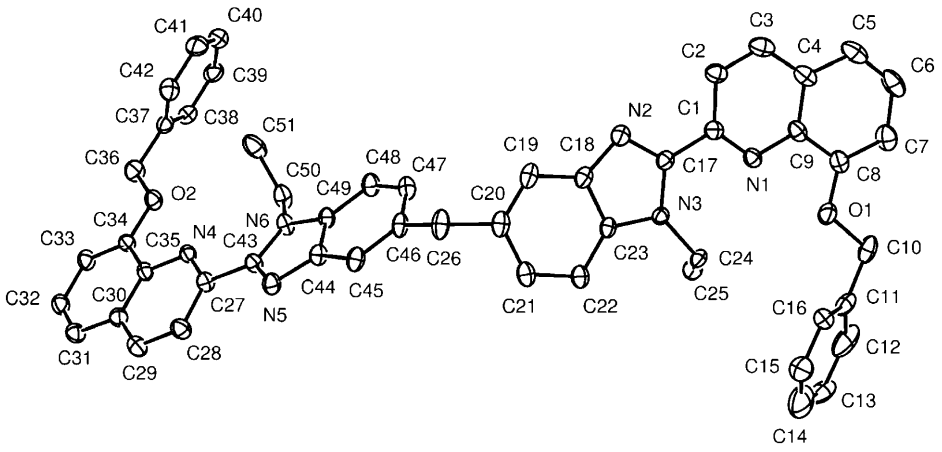

Figure 1. View of the crystal structure of the precursor ligand **7** with numbering scheme. Ellipsoids are represented at the 30% probability level.

$$H = 6\sqrt{3\pi}\frac{LA}{D^3} \qquad (4)$$

Synthesis and structure of the complexes $[Ln_2(L12b\text{-}2H)_3]$ in the solid state: Reaction of the C_{2v}-symmetrical bis-tridentate ligand **L12b** (3 equiv) with $Ln(OTf)_3 \cdot x H_2O$ (2 equiv; Ln = La, Nd, Eu; $OTf^- = CF_3SO_3^-$ = triflate; x = 1–3) in acetonitrile containing K_2CO_3, followed by precipitation with diethyl ether, yields pure red-orange binuclear complexes $[Ln_2(\mathbf{L12b}\text{-}2H)_3] \cdot x H_2O$ (Table S4 in the Supporting Information). More than two

hundred crystallization attempts provided some extremely fragile red crystals, from which an X-ray crystal structure of limited quality (see the Experimental Section) could be eventually obtained (Figure 2, Table 1; and Tables S5–S7 in the Supporting Information).

Two independent neutral binuclear triple-stranded helical complexes possessing opposite helicities A-[Nd_2(**L12b**-2H)$_3$] (multiplicity: 8) and B-[Nd_2(**L12b**-2H)$_3$] (multiplicity: 4) are found in the unit cell, together with interstitial solvent molecules, thus leading to the complete chemical formula {A-[Nd_2(**L12b**-2H)$_3$]}$_2$·{B-[Nd_2(**L12b**-2H)$_3$]}·8CH_3CN·4H_2O (**10**) with $Z=4$. Although B-[Nd_2(**L12b**-2H)$_3$] is located on a crystallographic twofold axis passing through C19e, the metric of the two independent complexes is very similar (Table 1; Tables S5–S7 in the Supporting Information); they show pseudo-D_3 symmetrical binuclear triple-stranded helicates. The two metallic cations Nd^{III} are nine-coordinated in pseudo-tricapped trigonal prismatic sites, with each *HHH* site being defined by three oxygen atoms of the terminal phenol rings (upper tripod, average Nd–O_{phenol} = 2.40(1) Å), three capping nitrogen atoms of the quinolines (average Nd–N_{quin} = 2.65(1) Å), and three nitrogen atoms of the benzimidazole rings (lower tripod, average Nd–N_{bzim} = 2.72(1) Å; Table 1, Figure 2; and Scheme S2 in the Supporting Information). The Nd–O and the Nd–N bond lengths are comparable to those reported for the mononuclear complex *HHT*-[Nd(**L10**-H)$_3$] (R = Me in Scheme 2; average Nd–O_{phenol} = 2.406(8) Å, average Nd–N_{quin} = 2.64(2) Å, and average Nd–N_{bzim} = 2.73(6) Å).[12] This logically leads to the calculation of similar nine-coordinate ionic radii randomly distributed around the values of 1.163 Å that are expected for unconstrained nine-coordinate Nd^{III}.[26] We thus deduce that 1) the different relative orientations of the three 2-benzimidazol-8-hydroxyquinoline binding units bound to Nd^{III} (*HHH* or *HHT*), and 2) the incorporation of the benzimidazole ring into the diphenylmethane spacer in [Nd_2(**L12b**-2H)$_3$] has no major structural effect in the final complexes. However, the average bond valences,[27,28] which reflects the strength of the Ln–donor interactions,[29] provide evidence for stronger interactions for the terminal oxygen atoms in [Nd_2(**L12b**-2H)$_3$] at the cost of some weaker interactions with the nitrogen atoms of the benzimidazole rings, thus maintaining the bond-valence sum within the acceptable range of $V_{Nd}=3.0\pm0.2$ (Table 1).[30] Comparison with [Tb_2(**L3**-2H)$_3$], in which the terminal-fused hydroxyquinoline rings are replaced with pyridine–carboxylate units (Schemes 1 and 2), shows the opposite trend with a smaller difference between $\nu_{Ln,O}$ and $\nu_{Ln,Nbzim}$ (Table 1). An analysis

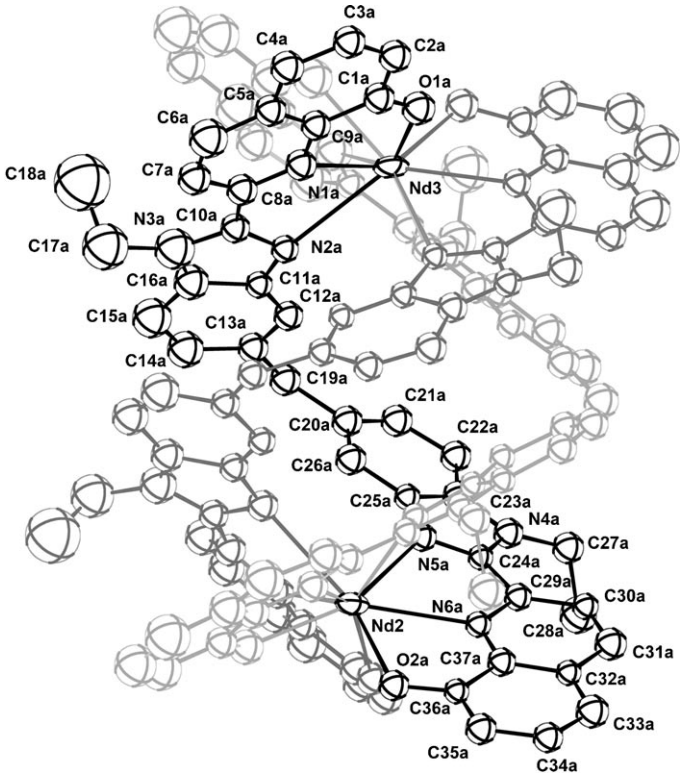

Figure 2. Perspective view with numbering scheme of the molecular structure of A-[Nd_2(**L12b**-2H)$_3$] in the crystal structure of **10**. Ellipsoids are represented at 30% probability level. The three strands are represented with different grayscale intensities (the respective strands are named a, b, and c for A-[Nd_2(**L12b**-2H)$_3$], and d, e, and f for B-[Nd_2(**L12b**-2H)$_3$]).

Table 1. Ln–Ln distances, average Ln–N and Ln–O bond lengths [Å], bond valences ($\nu_{Ln,j}$),[a] bond-valence sums (V_{Ln}),[b] and geometric analysis of the coordination polyhedra in A-[Nd_2(**L12b**-2H)$_3$] and B-[Nd_2(**L12b**-2H)$_3$] helicates and related complexes.

Compound		Ln–N[c]		Ln–O[c]	Ln···Ln	$\nu_{Ln,N}$[c]		$\nu_{Ln,O}$[c]	V_{Ln}	Ref.
		Bzim[d]	Quin[d]			Bzim[d]	Quin[d]			
A-[Nd_2(**L12b**-2H)$_3$]	Nd2	2.72(6)	2.66(3)	2.41(1)	9.021(2)	0.25(3)	0.29(2)	0.413(6)	2.84	this work
	Nd3	2.71(4)	2.63(1)	2.41(2)	–	0.25(3)	0.314(8)	0.42(3)	2.96	this work
B-[Nd_2(**L12b**-2H)$_3$]	Nd1	2.73(3)	2.65(1)	2.39(1)	9.047(2)	0.24(2)	0.30(4)	0.44(5)	2.94	this work
A-[Tb_2(**L3**-2H)$_3$]	Tb1 A	2.60(1)	2.55(1)	2.37(2)	8.829(1)	0.285(5)	0.32(1)	0.39(3)	2.97	[3a]
	Tb2 A	2.62(1)	2.56(2)	2.36(1)	–	0.31(2)	0.266(9)	0.394(7)	2.92	
B-[Tb_2(**L3**-2H)$_3$]	Tb1 B	2.61(1)	2.54(2)	2.37(5)	9.069(1)	0.271(9)	0.33(1)	0.38(5)	2.95	[3a]
	Tb2 B	2.60(4)	2.52(1)	2.39(3)	–	0.353(4)	0.28(4)	0.37(3)	2.99	
[Tb_2(**L2**)$_3$]$^{6+}$	Tb1	2.56(1)	2.57(3)	2.36(4)	9.06(3)	0.31(1)	0.31(3)	0.39(4)	3.03	[2a]
	Tb2	2.59(5)	2.59(3)	2.36(3)	–	0.29(4)	0.29(2)	0.39(3)	2.91	

[a] $\nu_{Ln,j}=e^{[(R_{Ln,j}-d_{Ln,j})/b]}$, in which $d_{Ln,j}$ is the Ln–donor atom j distance. The bond-valence parameters $R_{Ln,N}$ and $R_{Ln,O}$ are taken from ref. [28] and b = 0.37 Å.[27] [b] $V_{Ln}=\sum_j \nu_{Ln,j}$.[28] [c] Each value is the average of three bond lengths and the number in parentheses corresponds to the standard deviation of the average. The original uncertainties affecting each bond length are given in Table S5 in the Supporting Information. [d] Bzim = benzimidazole and Quin = quinoline.

of the geometries, shapes and helicities of these two complexes shows very similar characteristics (Tables S8 and S9, and Figures S2 and S3 in the Supporting Information). Consequently, the Nd···Nd contact distance in the $[Nd_2(\mathbf{L12b}\text{-}2H)_3]$ (9.02–9.05 Å) is almost identical to those found in $[Tb_2(\mathbf{L3}\text{-}2H)_3]$ and $[Tb_2(\mathbf{L2})_3]^{6+}$ (Table 1), thus leading to approximate palindromic helices (length $\approx$1.4 nm, diameter $\approx$1.1 nm, pitch $\approx$1.4 nm per turn).

Interestingly, reaction of the **L12b** (3 equiv) with $Ln(OTf)_3{\cdot}x\,H_2O$ (2 equiv; Ln = Y, Lu; x = 1–3) in acetonitrile containing K_2CO_3 failed to give pure binuclear complexes $[Ln_2(\mathbf{L12b}\text{-}2H)_3]{\cdot}x\,H_2O$, which are systematically contaminated with 15–25% of the highly insoluble complexes $[Ln_2(\mathbf{L12b}\text{-}2H)_2(OTf)_2]$ that possess Ln/**L12** = 2:2 stoichiometry (Table S4 in the Supporting Information).

Speciation, stability, and structure of the complexes $[Ln_2(\mathbf{L12b}\text{-}2H)_3]$ in solution: The faint solubility of both free ligand **L12b** and of its complexes $[Ln_2(\mathbf{L12b}\text{-}2H)_3]$ in water or in polar organic solvent represents a severe handicap for the characterization of the assembly processes operating in solution. After considerable effort, we found that titrations of the deprotonated ligand $[\mathbf{L12b}\text{-}2H]^{2-}$ (obtained from reaction of **L12b** with 2 equiv of $(n\mathrm{Bu})_4\mathrm{NOH}$) with increasing quantities of $Ln(OTf)_3{\cdot}x\,H_2O$ (Ln = La, Nd, Eu, Y, Lu; x = 1–3) can be performed at 10^{-4} M in CH_2Cl_2/CH_3OH (1:1), or up to 2×10^{-3} M in DMSO, although the pure deprotonated ligand rapidly (within one hour) decomposes in the latter solvent. Monitoring the titrations with electrospray ionization mass spectrometry (ESIMS) for Ln/**L12b** in the range 0.1 to 2.0 displays similar results in both solvents and shows the successive formation of three charged complexes $[Ln_2(\mathbf{L12b}\text{-}2H)_3{+}2H]^{2+}$ (Ln/**L12b** = 0.67), $[Ln_2(\mathbf{L12b}\text{-}2H)_2]^{2+}$ (Ln/**L12b** = 1.0), and $[Ln_2(\mathbf{L12b}\text{-}2H)(OTf)_3(H_2O)_4(CH_3OH)_4]^{+}$ (Ln/**L12b** = 2.0), together with some adducts of these complexes with either solvent molecules or counterions (Figure S4 and Tables S10–S14 in the Supporting Information). For the large lanthanides (Ln = La, Nd, Eu), the ESIMS spectra recorded for Ln/**L12b** $\leq$ 1.0 were dominated by the signal of the doubly protonated complex $[Ln_2(\mathbf{L12b}\text{-}2H)_3{+}2H]^{2+}$ (Figure S4a), which is probably obtained by the fixation of protons onto the terminal negatively charged phenol tripods of the triple helix, as previously described for K^+ in the crystal structure of *HHH*-$[Er(\mathbf{L8}\text{-}H)_3{+}K]^{+}$.[10b] Further addition of metal (Ln/**L12b** $\geq$ 1.0) yields the formation of $[Ln_2(\mathbf{L12b}\text{-}2H)_2]^{2+}$ at the expense of $[Ln_2(\mathbf{L12b}\text{-}2H)_3{+}2H]^{2+}$. For the smaller lanthanides (Ln = Y, Lu), the competition between $[Ln_2(\mathbf{L12b}\text{-}2H)_3{+}2H]^{2+}$ and $[Ln_2(\mathbf{L12b}\text{-}2H)_2]^{2+}$ is more pronounced (Figure S4b), whereas in an excess of metal, we detect signals diagnostic of the formation of an unsaturated 2:1 complex $[Ln_2(\mathbf{L12b}\text{-}2H)(OTf)_3(H_2O)_4(CH_3OH)_4]^{+}$, for which the ESIMS response is expected to be weak.[31]

Parallel spectrophotometric titrations of $[\mathbf{L12b}\text{-}2H]^{2-}$ with $Ln(OTf)_3{\cdot}x\,H_2O$ performed at 2×10^{-4} M in CH_2Cl_2/CH_3OH (1:1) show a complicated variation of both ligand-centered $\pi\rightarrow\pi^*$ transitions (250–380 nm) and intraligand charge-transfer (ILCT) transitions (400–500 nm),[12] which result from the complexation of the tridentate N_2O^- binding units to Ln^{3+} (Figure 3). We observe two end points around Ln/**L12b** = 0.67 and Ln/**L12b** = 1.0, followed by a smooth evolution for Ln/**L12b** > 1.0, which is almost negligible for large lanthanides (Ln = La, Nd, Eu; Figure 3a) but very significant for small lanthanides (Ln = Y, Lu; Figure 3b). Factor analyses[32] suggest the formation of, respectively, three (large Ln^{III}) or four (small Ln^{III}) absorbing species during the titration processes, and the spectrophotometric data can be satisfyingly fitted with the equilibria shown in Equations (5) and (6) for Ln = La, Nd, Eu, and Equations (5)–(7) for Ln = Y, Lu, by using nonlinear least-squares techniques.[33]

$$3\,[\mathbf{L12b}\text{-}2H]^{2-} + 2\,Ln^{3+} \rightleftharpoons [Ln_2(\mathbf{L12b}\text{-}2H)_3] \quad \beta_{2,3}^{Ln,L12b} \qquad (5)$$

$$2\,[\mathbf{L12b}\text{-}2H]^{2-} + 2\,Ln^{3+} \rightleftharpoons [Ln_2(\mathbf{L12b}\text{-}2H)_2]^{2+} \quad \beta_{2,2}^{Ln,L12b} \qquad (6)$$

$$[\mathbf{L12b}\text{-}2H]^{2-} + 2\,Ln^{3+} \rightleftharpoons [Ln_2(\mathbf{L12b}\text{-}2H)]^{4+} \quad \beta_{2,1}^{Ln,L12b} \qquad (7)$$

The associated cumulative constants $\log(\beta_{2,3}^{Ln,L12b})$ and $\log(\beta_{2,2}^{Ln,L12b})$ collected in Table 2 are of the same magnitude as those previously reported for $[Ln_2(\mathbf{L11}\text{-}2H)_3]$ and $[Ln_2(\mathbf{L11}\text{-}2H)_2]^{2+}$ in acetonitrile (Ln = Eu, Yb),[13] but we detect some selectivity with a preference for the fixation of mid-range lanthanides (Table 2; Figure S5 in the Supporting Information).

Interestingly, the stabilities of $[Ln_2(\mathbf{L12b}\text{-}2H)_3]$ and $[Ln_2(\mathbf{L12b}\text{-}2H)_2]^{2+}$ for Ln = Nd and Lu are comparable, but the possibility for the smaller lanthanide to form the stable $[Lu_2(\mathbf{L12b}\text{-}2H)]^{4+}$ complex limits the formation of the triple helix (Figure 4), which partly explains the difficulties encountered in isolating pure neutral complexes along the second part of the lanthanide series.

^{1}H NMR spectroscopic data are especially hard to obtain because of the poor sensitivity of this technique, which usually requires concentrations in the millimolar range. Solubility of both ligands and complexes in CD_2Cl_2/CD_3OH (1:1) is not sufficient, but reliable ^{1}H NMR spectra can be recorded for saturated solutions of $[Ln_2(\mathbf{L12b}\text{-}2H)_3]$ in CD_3CN with the larger lanthanides (Ln = La, Nd, Eu, Y), whereas titrations cannot be envisioned because of precipitation of $[Ln_2(\mathbf{L12b}\text{-}2H)_2](OTf)_2$ in an excess of metal. The ^{1}H NMR spectra of both diamagnetic (Ln = La, Y; Figure 5) and fast-relaxing paramagnetic (Ln = Nd, Eu; Figure S6 in the Supporting Information) $[Ln_2(\mathbf{L12b}\text{-}2H)_3]$ complexes display eight signals for the aromatic protons, which are diagnostic for D_3 (helical) or C_{3h} symmetry (side-by-side).[34] The concomitant observation of singlets (i.e., A_2 spin systems) for the enantiotopic methylene protons of the diphenylmethane spacer (H9,9′ in Figure 5) requires three twofold axes perpendicular to the threefold axis and thus confirms the formation of the expected D_3-symmetrical triple helix.[35] A complete assignment is obtained by means of 2D-COSY and 2D-NOESY spectroscopies for the diamagnetic complexes, although some ambiguities remain for the paramagnetic an-

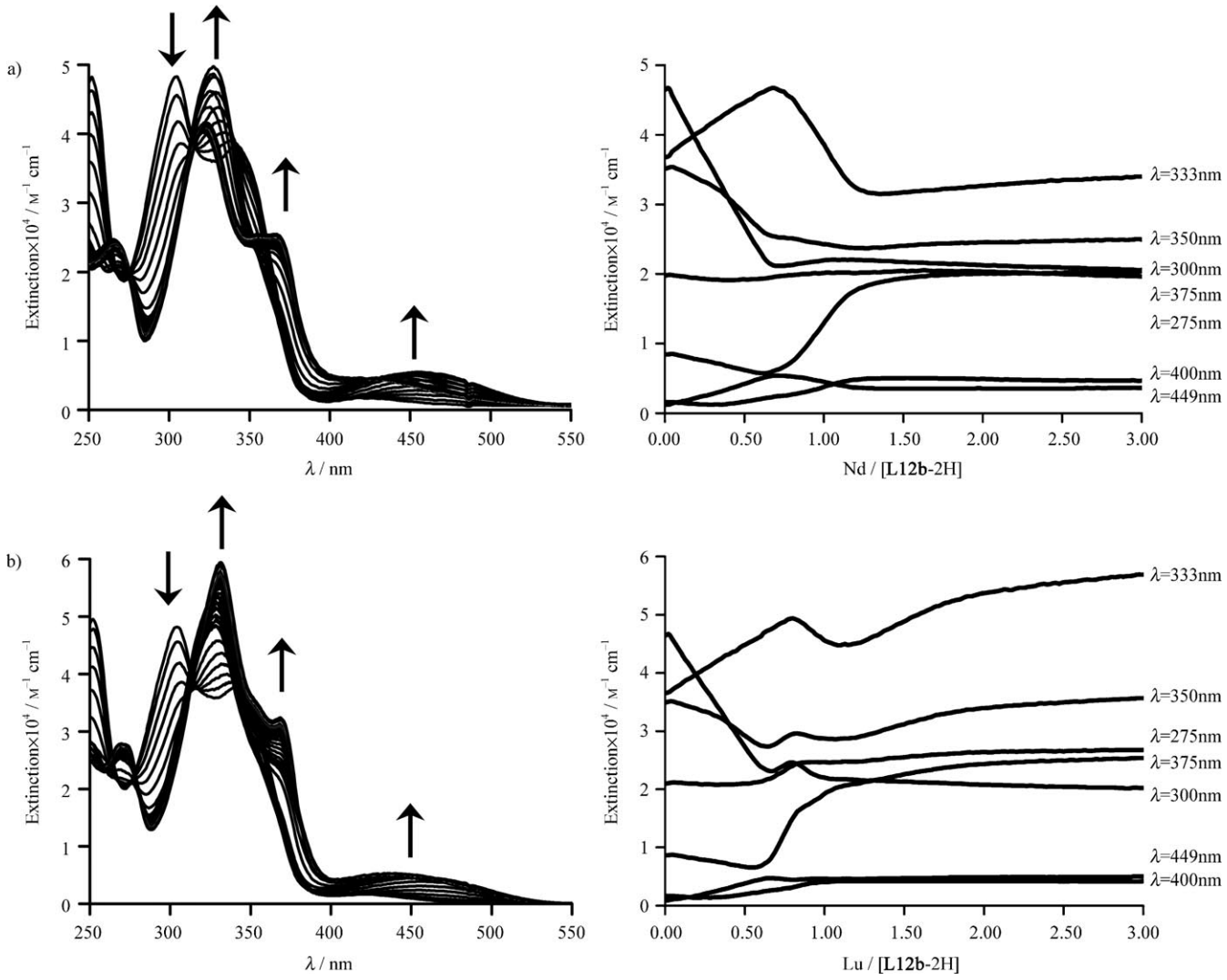

Figure 3. Variation of the absorption spectra and corresponding variations of molar extinctions at seven different wavelengths observed for the spectrophotometric titrations of $[\mathbf{L12b}\text{-}2H]^{2-}$ (2×10^{-4} M in CH_2Cl_2/MeOH 1:1) with a) $Nd(OTf)_3$ and b) $Y(OTf)_3$ (Ln/**L12b** = 0.1–3.0).

alogues since the increased nuclear relaxation severely limits the use of these two-dimensional techniques (Figure S6 in the Supporting Information).

In the more coordinating [D$_6$]DMSO solvent, the stability constants are severely reduced and we observe a significant amount of free ligand in slow exchange with $[Ln_2(\mathbf{L12b}\text{-}2H)_3]$ for Ln/**L12b** = 0.67 and a total ligand concentration of 2×10^{-3} M (Ln = La, Nd, Eu, Y, Lu; Figures S7–S11 in the Supporting Information). However, the addition of an excess of metal does not produce immediate precipitation and we can record the ^{1}H NMR spectroscopic signatures for the successive formation of $[Ln_2(\mathbf{L12b}\text{-}2H)_2]^{2+}$ and $[Ln_2(\mathbf{L12b}\text{-}2H)]^{4+}$. For large diamagnetic (Ln = La) or paramagnetic (Ln = Nd, Eu) lanthanides, the broadened signals due to intermediate chemical exchange on the NMR spectroscopic timescale, combined with lanthanide-induced relaxation, prevent a detailed analysis. On the other hand, the ^{1}H NMR spectroscopic titrations with small diamagnetic cations (Ln = Y, Lu; Figures S10 and S11) show the stepwise replacement of the D_3-symmetrical $[Ln_2(\mathbf{L12b}\text{-}2H)_3]$ helicate with $[Ln_2(\mathbf{L12b}\text{-}2H)_2]^{2+}$ existing as a mixture of double-stranded (D_2 symmetry characterized by enantiotopic H9,9′ and diastereotopic H10,10′ methylene protons)[34] and side-by-side (C_{2h} symmetry characterized by two diastereotopic pairs of methylene protons for H9,9′ and H10,10′, Scheme 4a),[34] a situation previously documented for related binuclear lanthanide complex with bis-bidentate Schiff base ligands.[36] The ultimate complex $[Ln_2(\mathbf{L12b}\text{-}2H)]^{4+}$ displays ^{1}H NMR spectroscopic singlet signals for all methylene probes H9,9′ and H10,10′, which is in line with an average extended planar C_{2v} symmetry of the ligand strand (Scheme 4b) previously established for the related complexes $[Ln_2(\mathbf{L2})(NO_3)_6]$.[25]

Thermodynamic modeling and rationalization of the formation of the complexes $[Ln_2(\mathbf{L12b}\text{-}2H)_n]^{(6-2n)+}$ (n = 1–3) in solution: The application of the site-binding model [Eq. (3)] to the complexation equilibria in Equations (5)–(7) yields

Table 2. Experimental and computed cumulative formation constants $\log(\beta_{1,n}^{Ln,L10b})$ and $\log(\beta_{2,n}^{Ln,L12b})$ obtained by spectrophotometry according to the equilibria in Equations (5)–(7) and (11)–(13) for the complexes $[Ln_2(\mathbf{L12b}\text{-}2H)_n]^{(6-2n)+}$ and $[Ln(\mathbf{L10b}\text{-}2H)_n]^{(3-2n)+}$ (Ln = La, Nd, Eu, Y, and Lu; CH_2Cl_2/CH_3OH 1:1, 298 K).

Ln^{III}		La	Nd	Eu	Y	Lu
$R_{Ln}^{CN=9}$[Å][a]		1.216	1.163	1.120	1.075	1.032
$\log(\beta_{2,3}^{Ln,L12b})$	exptl[b]	23.1(6)	24.8(5)	27.0(8)	26.5(5)	24.0(4)
	calcd1[c]	23.1	24.8	27.0	26.8	24.3
	calcd2[d]	–	–	–	26.5	24.0
$\log(\beta_{2,2}^{Ln,L12b})$	exptl[b]	17.0(5)	18.7(4)	20.2(7)	20.9(4)	18.6(3)
	calcd1[c]	17.0	18.7	20.2	20.4	18.1
	calcd2[d]	–	–	–	20.9	18.6
$\log(\beta_{2,1}^{Ln,L12b})$	exptl[b]	≤ 10	≤ 11	≤ 12	13.0(3)	11.7(2)
	calcd1[c]	*12.9*	*13.8*	*14.8*	13.2	12.0
	calcd2[d]	–	–	–	13.0	11.7
$\log(\beta_{1,3}^{Ln,L10b})$	exptl[b]	20.3(5)	19.7(5)	20.1(6)	23.1(9)	23.5(9)
	calcd1[c]	20.3	19.7	20.1	23.4	23.7
	calcd2[d]	–	–	–	23.1	23.5
$\log(\beta_{1,2}^{Ln,L10b})$	exptl[b]	14.8(4)	14.2(4)	14.5(5)	16.0(9)	16.6(6)
	calcd1[c]	14.9	14.1	14.5	15.6	16.3
	calcd2[d]	–	–	–	15.8	16.5
$\log(\beta_{1,1}^{Ln,L10b})$	exptl[b]	8.3(3)	7.6(6)	7.9(3)	8.0(6)	8.7(7)
	calcd1[c]	8.2	7.7	7.9	7.9	8.5
	calcd2[d]	–	–	–	8.2	8.8
AF_{Ln}[e]	calcd1[c]	0.0023	0.0017	0.0006	0.0171	0.0180
	calcd2[d]	–	–	–	0.0050	0.0025

[a] Ionic radii for nine-coordinate trivalent lanthanides.[26] [b] The quoted errors correspond to those estimated during the nonlinear least-square fits. [c] Computed with Equations (8)–(10) and (14)–(16) and parameters of Table 3 (first fitting process). [d] Computed with Equations (8)–(9) and (14)–(17) and parameters of Table 3 (second fitting process). [e] Willcott agreement factor; see text and references.[38]

Equations (8)–(10), in which the three experimentally accessible thermodynamic constants $\beta_{2,3}^{Ln,L12b}$, $\beta_{2,2}^{Ln,L12b}$, and $\beta_{2,1}^{Ln,L12b}$ require a minimal set of four microscopic parameters for their modeling ($f_{N_2O}^{Ln,L12b}$ is the affinity, including desolvation, of Ln^{III} for the tridentate binding site in $[\mathbf{L12b}\text{-}2H]^{2-}$; $u^{Ln,Ln}$ and $u^{L,L}$ are the average Boltzmann factors for intramolecular homo-component interactions operating within the final assemblies; and c^{eff} is the average effective concentration characterizing the macrocyclization processes responsible for the formation of discrete double-stranded or triple-stranded helicates), together with a statistical factor calculated by using the method of symmetry numbers, first introduced by Benson (detailed calculations are given in the Supporting Information).[14,37]

$$\beta_{2,3}^{Ln,L12b} = 96(f_{N_2O}^{Ln,L12b})^6(c^{eff})^2(u^{L,L})^6(u^{Ln,Ln}) \quad (8)$$

$$\beta_{2,2}^{Ln,L12b} = 72(f_{N_2O}^{Ln,L12b})^4(c^{eff})(u^{L,L})^4(u^{Ln,Ln}) \quad (9)$$

$$\beta_{2,1}^{Ln,L12b} = 36(f_{N_2O}^{Ln,L12b})^2(u^{Ln,Ln}) \quad (10)$$

The collection of a sufficient number of experimental stability constants forced us to perform additional spectrophotometric titrations of the simple tridentate ligands $[\mathbf{L10b}\text{-}H]^-$ with $Ln(OTf)_3{\cdot}xH_2O$ (2×10^{-4} M in CH_2Cl_2/CH_3OH (1:1), 298 K); these eventually give three additional macroconstants $\beta_{1,3}^{Ln,L10b}$, $\beta_{1,2}^{Ln,L10b}$, and $\beta_{1,1}^{Ln,L10b}$, which correspond to the equilibria in Equations (11)–(13) after nonlinear least-squares fits of the data (Table 2).[33]

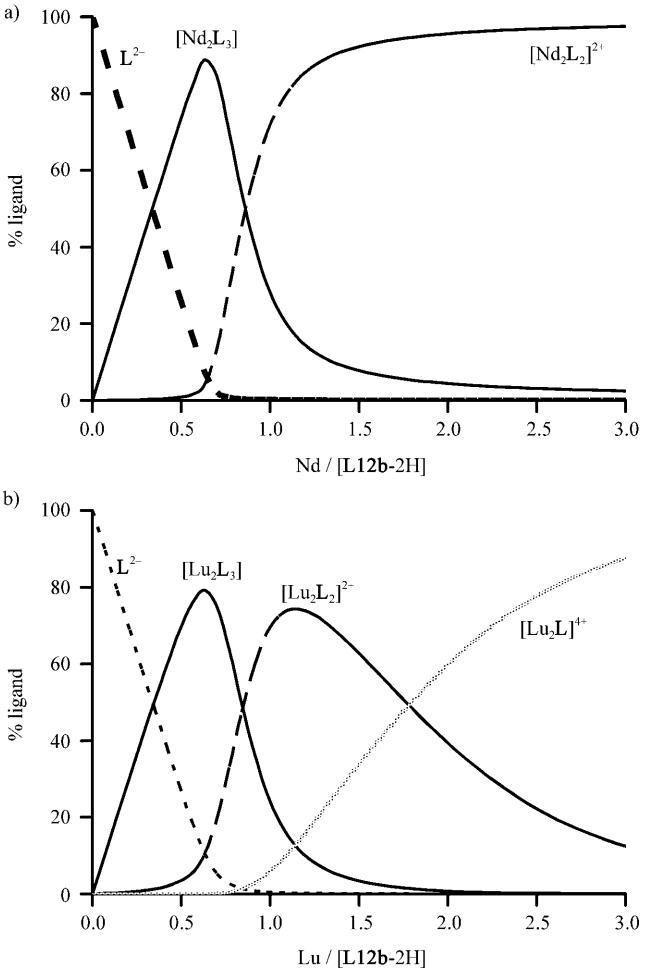

Figure 4. Computed speciation (% ligand) for the titration of 2×10^{-4} M $[\mathbf{L12b}\text{-}2H]^{2-}$ with a) $Nd(OTf)_3$ and b) $Lu(OTf)_3$ (stability constants are taken from Table 2, CH_2Cl_2/MeOH 1:1).

$$3\,[\mathbf{L10b}\text{-}H]^- + Ln^{3+} \rightleftharpoons [Ln(\mathbf{L10b}\text{-}H)_3] \quad \beta_{1,3}^{Ln,L10b} \quad (11)$$

$$2\,[\mathbf{L10b}\text{-}H]^- + Ln^{3+} \rightleftharpoons [Ln(\mathbf{L10b}\text{-}H)_2]^+ \quad \beta_{1,2}^{Ln,L10b} \quad (12)$$

$$[\mathbf{L10b}\text{-}H]^- + Ln^{3+} \rightleftharpoons [Ln(\mathbf{L10b}\text{-}H)]^{2+} \quad \beta_{1,1}^{Ln,L10b} \quad (13)$$

To limit the number of adjustable microscopic parameters, we have set 1) $u_{HH}^{L,L} = u_{HT}^{L,L} = u^{L,L}$, which implies statistical distributions of the microspecies *HH*-$[Ln(\mathbf{L10b}\text{-}H)_2]^+$/*HT*-$[Ln(\mathbf{L10b}\text{-}H)_2]^+ = 1.0$ and *HHH*-$[Ln(\mathbf{L10b}\text{-}H)_3]$/*HHT*-$[Ln(\mathbf{L10b}\text{-}H)_3] = 0.33$ (justified by the similar Nd–N and Nd–O bond lengths and bond valences found in *HHT*-$[Nd(\mathbf{L10b}\text{-}H)_3]$ and (*HHH*)-$[Nd_2(\mathbf{L12b}\text{-}2H)_3]$ in the solid state), and 2) $f_{N_2O}^{Ln,L10b} = f_{N_2O}^{Ln,L12b}$ (i.e., the tridentate binding units in $[\mathbf{L10b}\text{-}H]^-$ and $[\mathbf{L12b}\text{-}H]^{2-}$ have similar affinities for Ln^{III}). Application of the site-binding model [Equa-

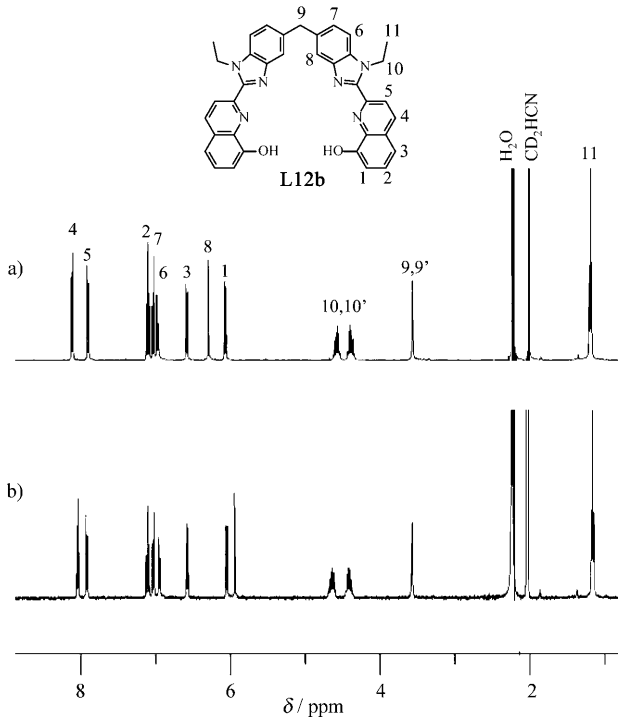

Figure 5. ^{1}H NMR spectra with numbering scheme for diamagnetic triple-stranded helicates a) $[La_2(\mathbf{L12b}\text{-}2H)_3]$ and b) $[Y_2(\mathbf{L12b}\text{-}2H)_3]$ (CD_3CN, 298 K).

tion (3)] eventually gives Equations (14)–(16).

$$\beta_{1,3}^{Ln,L10b} = 16(f_{N_2O}^{Ln,L12b})^3(u^{L,L})^3 \quad (14)$$

$$\beta_{1,2}^{Ln,L10b} = 12(f_{N_2O}^{Ln,L12b})^2(u^{L,L}) \quad (15)$$

$$\beta_{1,1}^{Ln,L10b} = 6(f_{N_2O}^{Ln,L12b}) \quad (16)$$

Simultaneous multilinear least-squares fits of Equations (8)–(10) and (14)–(16) for each lanthanide yield the sets of four microscopic thermodynamic descriptors collected in Table 3 (rows 1–8) and shown in Figure 6a, which satisfyingly reproduce the experimental data, as ascertained by the small computed values of the Willcott agreement factors ($0.0006 \leq AF_{Ln} \leq 0.0180$, Table 2).[38]

The main driving force of the complexation processes results from intermolecular metal–ligand connection processes, which do not significantly vary along the lanthanide series ($-44 \leq \Delta G_{inter}^{Ln,L12b} \leq -39\ kJ\,mol^{-1}$). The interligand interactions also poorly change along the lanthanide series, but contribute to a global destabilization ($\Delta E^{L,L} \geq 0$) when the metals are stepwise saturated with tridentate binding units. The concave behavior of $\Delta E^{Ln,Ln}$, which shows a minimum intermetallic repulsion for mid-range Ln^{III} (Figure 6a), is responsible for the parallel extra stabilization of the binuclear $[Ln_2(\mathbf{L12b}\text{-}2H)_n]^{(6-2n)+}$ complexes ($n=2$, 3) in the middle of the series (Table 2; Figure S5 in the Supporting Information).

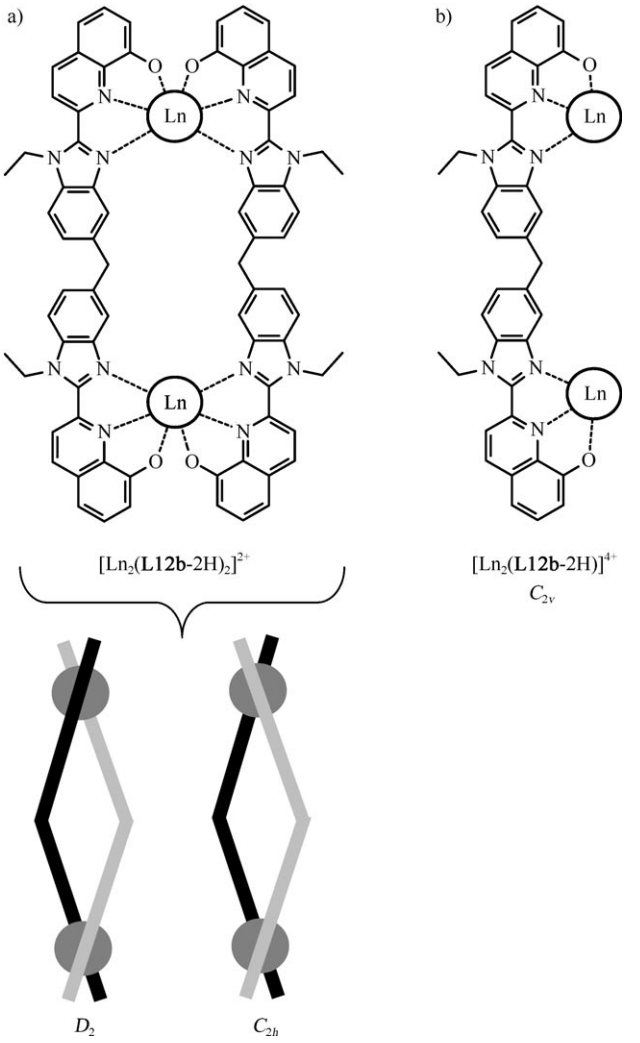

Scheme 4. Schematic representations of the solution structures established by ^{1}H NMR spectroscopy for a) $[Ln_2(\mathbf{L12b}\text{-}2H)_2]^{2+}$ existing as a mixture of helical (D_2 symmetry) and side-by-side (C_{2h} symmetry) double-stranded complexes, and b) $[Ln_2(\mathbf{L12b}\text{-}2H)]^{4+}$ (average C_{2v} symmetry on the NMR spectroscopic timescale). The coordination spheres of Ln^{III} have not been saturated with solvent molecules for the sake of clarity.

However, the most striking point concerns the very low effective concentrations[39] ($-9 \leq \log(c^{eff}) \leq -6$), which is at least two orders of magnitude smaller than 1) $\log(c^{eff}) = -4.1(4)$ reported for $[Lu_2(\mathbf{Lk})_n]^{6+}$ in acetonitrile ($k=1$, 2, Scheme 1; $n=2$, 3),[19] and 2) $\log(c^{eff}) = -0.3(4)$, estimated from thermodynamic and kinetic data collected for $[Eu_m(\mathbf{L3}\text{-}2H)_n]^{(3m-2n)+}$ in water at pH 6.15.[15] Moreover, $\log(c^{eff})$ in $[Ln_2(\mathbf{L12b}\text{-}2H)_n]^{(6-2n)+}$ abruptly decreases in going from Ln = Eu to Ln = Y, which translates into an inversion of the sign of the free-energy change characterizing intramolecular macrocyclization processes ($\Delta G_{inter}^{Ln,L12b} < 0$ is favorable for large Ln^{III}, but $\Delta G_{intra}^{Ln,L12b} > 0$ is unfavorable for small Ln^{III}; Figure 6a). Although this factor may explain the limited stability of macro(bi)cyclic double-stranded and triple-stranded binuclear helicates with respect to the noncy-

Table 3. Fitted microscopic thermodynamic parameters for $[Ln(\mathbf{L10b}\text{-}H)_n]^{(3n)+}$ and $[Ln_2(\mathbf{L12b}\text{-}2H)_n]^{(6-2n)+}$ (Ln = La, Nd, Eu, Y, and Lu; CH_2Cl_2/CH_3OH 1:1, 298 K).[a]

Fitted parameters (first fit)[b]	La	Nd	Eu	Y	Lu
$\log(f_{N_2O}^{Ln,L12b})$	7.44(6)	6.87(5)	7.14(2)	7.1(4)	7.7(3)
$\Delta G_{inter}^{Ln,L}$ [kJ mol^{-1}][c]	−42.4(4)	−39.2(3)	−40.7(1)	−41(2)	−44(2)
$\log(c^{eff})$	−6.8(1)	−6.4(1)	−5.83(4)	−8.5(8)	−8.9(8)
$\Delta G_{intra}^{Ln,L12b}$ [kJ mol^{-1}][d]	−3.6(6)	−2.7(5)	−7.5(2)	8(3)	7(3)
$\log(u^{L,L})$	−1.09(8)	−0.70(6)	−0.86(2)	−0.3(4)	−0.2(4)
$\Delta E^{L,L}$ [kJ mol^{-1}][e]	6.2(5)	4.0(4)	4.9(1)	2(2)	1(2)
$\log(u^{Ln,Ln})$	−3.5(2)	−1.5(2)	−0.99(6)	−2.5(8)	−4.9(8)
$\Delta E^{Ln,Ln}$ [kJ mol^{-1}][f]	20(1)	9(1)	5.6(4)	15(5)	28(5)
Fitted parameters (second fit)[g]	**La**	**Nd**	**Eu**	**Y**	**Lu**
$\log(f_{N_2O}^{Ln,L12b})$	–	–	–	7.4(2)	7.99(8)
$\Delta G_{inter}^{Ln,L}$ [kJ mol^{-1}][c]	–	–	–	−42(1)	−45.6(5)
$\log(c^{eff})$	–	–	–	−9.1(4)	−9.5(5)
$\Delta G_{intra}^{Ln,L12b}$ [kJ mol^{-1}][d]	–	–	–	10(2)	8.6(8)
$\log(u^{L,L})$	–	–	–	−0.1(2)	−0.56(9)
$\Delta E^{L,L}$ [kJ mol^{-1}][e]	–	–	–	1(1)	3.2(6)
$\log(u^{Ln,Ln})$	–	–	–	−1.1(5)	−3.4(3)
$\Delta E^{Ln,Ln}$ [kJ mol^{-1}][f]	–	–	–	6(3)	19(2)
$\log(u_{single\ strand}^{Ln,Ln})$	–	–	–	−3.4(4)	−5.8(2)
$\Delta E_{single\ strand}^{Ln,Ln}$ [kJ mol^{-1}][e]	–	–	–	19(2)	33(1)

[a] The uncertainties correspond to those found during the multilinear least-square fits. [b] First fit: $f_{N_2O}^{Ln,L12b}$, c^{eff}, $u^{L,L}$, $u^{Ln,Ln}$ by using Equations (8)–(10) and (14)–(16). [c] $\Delta G_{inter}^{Ln,L12b} = -RT\ln(f_{N_2O}^{Ln,L12b})$. [d] $\Delta G_{intra}^{Ln,L12b} = -RT\ln(f_{N_2O}^{Ln,L12b}c^{eff})$. [e] $\Delta E^{L,L} = -RT\ln(u^{L,L})$. [f] $\Delta E^{Ln,Ln} = -RT\ln(u^{Ln,Ln})$. [g] Second fit: $f_{N_2O}^{Ln,L12b}$, c^{eff}, $u^{L,L}$, $u^{Ln,Ln}$, $u_{single\ strand}^{Ln,Ln}$ by using Equations (8)–(9) and (14)–(17).

clic $[Ln_2(\mathbf{L12b}\text{-}2H)]^{4+}$ complex, particularly for small Ln^{III}, it is not sufficient to justify the nondetection of the latter complexes for large Ln^{III} (compare experimental and computed (italic) values of $\beta_{2,1}^{Ln,L12b}$ for Ln = La, Nd, Eu in Table 2). Although the quantitative dissection of $\Delta E^{Ln,Ln}$ into the opposite contributions of intramolecular coulombic repulsion and favorable solvation energies is beyond the scope of this already massive contribution,[19] we expect that $\Delta E^{Ln,Ln}$ becomes more repulsive at longer distances (a very counterintuitive result from ref. [19]), and we have also demonstrated that the formation of the single-stranded complex $[Ln_2(\mathbf{L2})(NO_3)_3]$ is accompanied by the planarization of the ligand and an increase of approximately 30% of the intramolecular intermetallic distance, relative to that found in the parent helicate $[Ln_2(\mathbf{L2})_3]^{6+}$.[25] With this in mind, we have kept a single average intermetallic interaction $\Delta E^{Ln,Ln}$ for macro(bi)cyclic complexes, but introduced a specific values $\Delta E_{single\ strand}^{Ln,Ln}$ for $[Ln_2(\mathbf{L12b}\text{-}2H)]^{4+}$, which transforms Equation (10) into Equation (17).

$$\beta_{2,1}^{Ln,L12b} = 36(f_{N_2O}^{Ln,L12b})^2(u_{single\ strand}^{Ln,Ln}) \quad (17)$$

A second round of multilinear least-squares fits of Equations (8), (9), and (14)–(17) for Ln = Y, Lu obviously improves the quality of the fit, but indeed confirms the counterintuitive sequence $\Delta E_{single\ strand}^{Ln,Ln} > \Delta E^{Ln,Ln}$ (Table 3, rows 9–18; Figure S12 in the Supporting Information), which may now rationalize the low stability constants observed for $[Ln_2(\mathbf{L12b}\text{-}2H)]^{4+}$ with large Ln^{III}.

From this complete thermodynamic picture for the formation of $[Ln_2(\mathbf{L12b}\text{-}2H)_n]^{(6-2n)+}$, it is tempting to assign the huge decrease of $\log(c^{eff})$ in going from **L2** (Ln = Lu)[19] or $[\mathbf{L3}\text{-}2H]^{2-}$ (Ln = Eu)[15] to $[\mathbf{L12b}\text{-}2H]^{2-}$ (Ln = La, Nd, Eu, Y, Lu) to the replacement of flexible terminal pyridine–carboxy(amide or late) groups with fused ten-membered rigid aromatic 8-hydroxyquinolinates. To substantiate this hypothesis, we have repeated this complete thermodynamic analysis for the formation of $[Ln_2(\mathbf{L2})_n]^{6+}$ (n = 1–2)[2b] and $[Ln(\mathbf{L13})_n]^{3+}$ (n = 1–3) in acetonitrile along the lanthanide series. Equations (8), (9), and (14)–(16) still apply for fitting the experimental stability constants (Table S15 in the Supporting Information) to give the microscopic parameters shown in Figure 6b (Table S16 in the Supporting Information). Despite the use of two different solvents for imperious solubility reasons, we have indeed selected two systems (CH_2Cl_2/CH_3OH (1:1) and CH_3CN) with similar polarities, which allow a direct comparison of the different parameters. We immediately notice that the absolute magnitude of the various thermodynamic parameters are similar, whereas their variation along the lanthanide series differ in both systems (Figure 6). However, the larger and most striking discrepancy unambiguously concerns the gradual increase of the effective concentration along the series for **L2** ($10^{-7.3}$ M (Ln = La) $\le c^{eff} \le 10^{-4.3}$ M (Ln = Lu); Table S16), which contrasts with its parallel decrease for **L12b** ($10^{-6.8}$ M (Ln = La) $\ge c^{eff} \ge 10^{-9.5}$ M (Ln = Lu); Table 3). This translates into an opposite trend for $\Delta G_{intra}^{Ln,L} = \Delta G_{intra}^{Ln,L} - RT\ln(c^{eff})$ in Figure 6, and we can thus safely assign the extremely low values of the effective concentration (10^{-7}–10^{-9} M) in **L12b** to the loss of two degrees of rotational freedom, a factor that more severely affects the macrocyclization processes around smaller lanthanides.

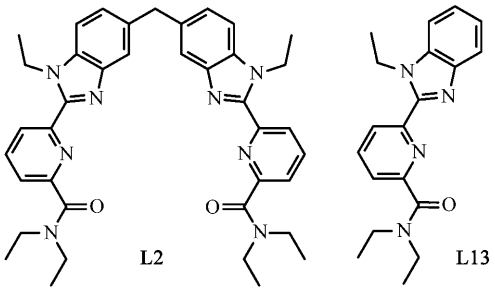

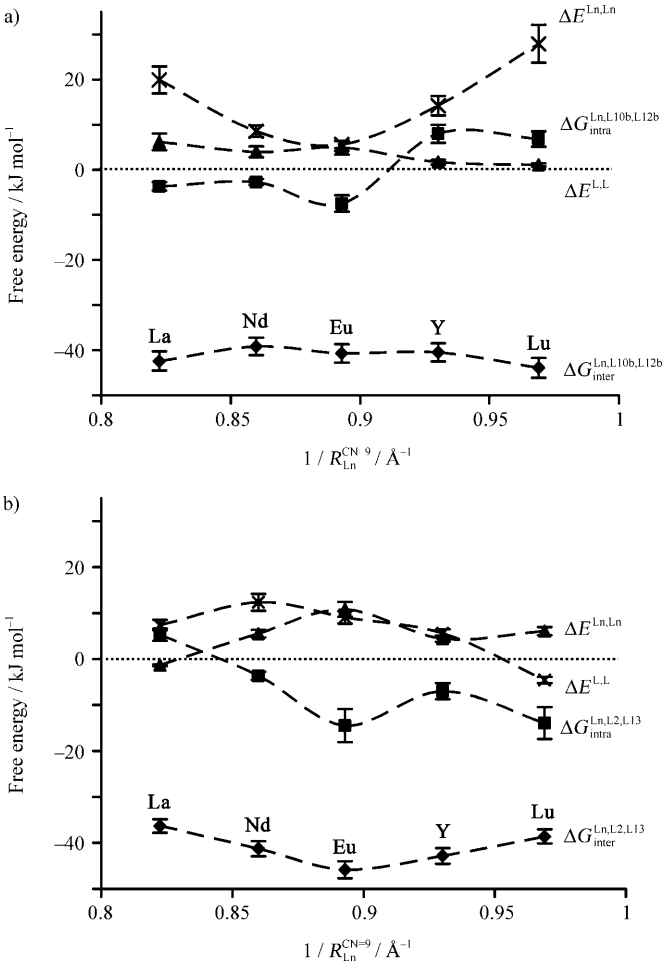

Figure 6. Plots of four microscopic thermodynamic parameters in the form of free energies of interactions, as a function of the inverse of nine-coordinate ionic radii for the assemblies of a) $[Ln(\mathbf{L10b}\text{-}H)_n]^{(3-n)+}$ and $[Ln_2(\mathbf{L12b}\text{-}2H)_n]^{(6-2n)+}$ ($n=1$–3, CH_2Cl_2/CH_3OH 1:1, 298 K), and b) $[Ln(\mathbf{L13})_n]^{3+}$ and $[Ln_2(\mathbf{L2})_n]^{6+}$ ($n=1$–3, CH_3CN, 298 K). The dotted lines are only guides for the eyes.

Conclusion

Reconsidering the specifications mentioned in the introduction, we have indeed established the structure of the triple-stranded binuclear helicates $[Ln_2(\mathbf{L12b}\text{-}2H)_3]$ and shown that it is similar to those of $[Ln_2(\mathbf{L3}\text{-}2H)_3]$ and $[Ln_2(\mathbf{L2})_3]^{6+}$ in the solid state and in solution, despite the fusion of the terminal aromatic rings in **L12b**. On the other hand, the thermodynamic assembly process is specific for each ligand strand, and is strongly influenced by the choice of the solvent. In weakly polar organic solvents, the free-energy changes in the connection of Ln^{3+} to an N_2O tridentate binding site are similar for $[\mathbf{L12b}\text{-}2H]^{2-}$ or **L2** ($\Delta G^{Ln,L12b}_{inter} = \Delta G^{Ln,L2}_{inter} \approx -42\ kJ\,mol^{-1}$), and we deduce that the huge contribution of charge neutralization to the entropy of complexation (through the relaxation of the organization of the solvent molecules),[16] is mainly restricted to water or to highly polar solvents, in which the formation of ionic pairs is negligible. For the $Ln^{3+}/[\mathbf{L12b}\text{-}2H]^{2-}$ system, we must consider that the respective counterions, $TfO^-/(n\mathrm{Bu})_4N^+$, have non-negligible interactions with their respective partners, and that their release into solution during the metal–ligand complexation process limits the classical charge-neutralization process described in water. This behavior may explain the decrease in stability by twenty-five orders of magnitude in going from $[Ln_2(\mathbf{L3}\text{-}2H)_3]$ (measured in water)[3] to $[Ln_2(\mathbf{L12b}\text{-}2H)_3]$ (measured in CH_2Cl_2/CH_3OH) or $[Ln_2(\mathbf{L11}\text{-}2H)_3]$ (measured in CH_3CN).[13] Beyond this crucial factor, the comparison of the assembly of the negatively charged segmental ligand $[\mathbf{L12b}\text{-}2H]^{2-}$ with that of its neutral analogue **L2**, performed in solvents of comparable polarities, shows that the effective concentration plays a leading role. Firstly, it decreases by approximately two orders of magnitude in going from **L2** to $[\mathbf{L12b}\text{-}2H]^{2-}$ because of the reduction of the total number of rotational degrees of freedom within the tridentate binding units that possess fused hydroxyquinoline groups. This eventually disfavors the macrocyclization processes that lead to $[Ln_2(\mathbf{L12b}\text{-}2H)_3]$. Secondly, the effective concentration decreases along the lanthanide series for $[\mathbf{L12b}\text{-}2H]^{2-}$, whereas it increases for **L2**, which produces opposite contributions to the quantities of linear over macrocyclic complexes formed along the series. This intimate dependence of the effective concentration on minor changes in the number of rotational degrees of freedom within the tridentate binding unit opens novel possibilities for rationally programming segmental ligands that favor the thermodynamic formation of discrete polynuclear complexes, or infinite coordination polymers,[40] with a predetermined number of bridging ligands—a strong point for the design of single-stranded lanthanide polymers extending along one direction and working as organic light-emitting diodes (OLEDs).[25] Finally, both $\Delta E^{L,L}$ and $\Delta E^{Ln,Ln}$ may bring some additional help for the fine thermodynamic tuning of the target assemblies. However, their physical origin arising from a balance between opposite and huge coulombic (repulsive) and solvation (attractive) interactions strongly limits their intuitive chemical programming.[18,19] In $[Ln_2(\mathbf{L12b}\text{-}2H)_3]$, the bowl-shaped curve found for $\Delta E^{Ln,Ln}$ is responsible for some variable contributions to the anti-cooperative processes, which eventually provides an extra stabilization for mid-range lanthanides, a remarkable behavior that could be exploited for producing heterometallic f–f systems that show some planned deviations from statistics.[41]

Experimental Section

General: Chemicals were purchased from Fluka AG and Aldrich and used without further purification unless otherwise stated. Starting synthons **4**,[21] **5**,[21] and ligands **L2**[2] and **L13**[25] were prepared according to literature procedures. The syntheses of intermediates **1**, **2**, and **3** were inspired from the literature,[20] but the modifications and improvements brought in this work justified a novel description of those three steps. The trifluoromethanesulfonate salts $Ln(CF_3SO_3)_3{\cdot}xH_2O$ were prepared from the corresponding oxide (Aldrich, 99.99%).[42] The Ln contents of solid salts were determined by complexometric titrations with Titriplex III (Merck) in the presence of urotropine and xylene orange.[43] Acetoni-

trile and dichloromethane were distilled over calcium hydride. Methanol was distilled over $Mg(OCH_3)_2$. Silica gel plates Merck 60 F254 were used for thin-layer chromatography (TLC) and Fluka silica gel 60 (0.04–0.063 mm) was used for preparative column chromatography.

Preparation of 1: 8-Hydroxyquinaldine (16.53 g, 103.84 mmol), benzyl bromide (26.64 g, 155.75 mmol), anhydrous K_2CO_3 (28.70 g, 207.66 mmol), and a catalytic amount of KI were suspended in acetone (150 mL), and heated at reflux until complete consumption of the starting materials (12 h, TLC: CH_2Cl_2/MeOH 98:2). The reaction mixture was evaporated to dryness and the residue dissolved in CH_2Cl_2/H_2O 1:1 (300 mL). The organic layer was separated and dried over anhydrous $MgSO_4$, filtered, and evaporated. The yellow oil was crystallized in hexane (200 mL/0 °C), filtered, washed with cold hexane, and dried for 24 h under vacuum to give **1** (20.50 g, 82.23 mmol, 79 %) as white crystals. ^{1}H NMR (400 MHz, $CDCl_3$): $\delta = 2.84$ (s, 3H), 5.49 (s, 2H), 7.02 (dd, $^3J = 7.6$ Hz, $^4J = 1.5$ Hz, 1H), 7.28–7.42 (m, 6H), 7.52–7.58 (m, 2H), 8.03 ppm (d, $^3J = 8.4$ Hz, 1H).

Preparation of 2: Compound **1** (15.00 g, 60.17 mmol) and SeO_2 (8.34 g, 75.16 mmol) were suspended in dioxane (120 mL). The white solid quickly dissolved and the color of the suspension turned red in a few minutes. The reaction mixture was then heated at 80 °C under an inert atmosphere. After 2 h, the suspension turned brown and no more starting material could be detected (TLC: CH_2Cl_2/MeOH 98:2). Selenium was filtered through Celite, and washed with dichloromethane. The yellow filtrate was evaporated, dried under vacuum for 12 h, redissolved in CH_2Cl_2 (100 mL), and kept at RT for 24 h. The red selenium precipitate was removed by filtration and the filtrate evaporated to dryness. The crude product was purified by column chromatography (silica gel, CH_2Cl_2/MeOH 100:0→99:1) to give **2** (13.05 g, 49.56 mmol, 83 %) as a yellow-brown solid. ^{1}H NMR (400 MHz, $CDCl_3$): $\delta = 5.52$ (s, 2H), 7.18 (d, $^3J = 7.8$ Hz, 1H), 7.33–7.61 (m, 7H), 8.09 (d, $^3J = 8.3$ Hz, 1H), 8.30 (d, $^3J = 8.3$ Hz, 1H), 10.35 ppm (s, 1H).

Preparation of 3: Compound **2** (10.00 g, 37.98 mmol) was dissolved in THF (250 mL), H_2O (175 mL) was added, and the pale yellow solution was cooled at 0 °C. H_2NSO_3H (14.75 g, 151.92 mmol) and $NaClO_2$ (13.74 g, 151.92 mmol) were added simultaneously and the color of the stirred solution rapidly turned orange. The complete consumption of the starting material required 30 min (TLC: CH_2Cl_2/MeOH 80:20). Water (1.5 L) was slowly added under sonication to precipitate a white solid, which was filtered, washed with water, and dried for 24 h under vacuum to give **3** (10.50 g, 37.88 mmol, 99 %) as a white solid. ^{1}H NMR (400 MHz, $CDCl_3$): $\delta = 5.38$ (s, 2H), 7.24 (dd, $^3J = 7.8$ Hz, $^4J = 1.2$ Hz, 1H), 7.37–7.65 (m, 7H), 8.32 (d, $^3J = 8.4$ Hz, 1H), 8.40 ppm (d, $^3J = 8.4$ Hz, 1H).

Preparation of 6: The reaction was carried out under a nitrogen atmosphere. A large excess of compound **3** (5.00 g, 27.89 mmol) was dissolved in dry CH_2Cl_2 (100 mL). Then, $SOCl_2$ (21.30 g, 179.04 mmol) and a catalytic amount of DMF (50 μL) were added. The solution changed from colorless to orange and a precipitate was formed. The reaction mixture was heated at reflux until the precipitate disappeared (1 h). The resulting solution was evaporated to dryness and the yellow solid was dried under vacuum at 80 °C for 1 h. This activated intermediate was dissolved in dry CH_2Cl_2 (75 mL), and compound **5** (2.06 g, 5.97 mmol) was added as a solid. The solution was heated at reflux for 1 h, at which point no starting material remained (TLC: CH_2Cl_2/MeOH 98:2). The pH of the reaction was adjusted to 7 by addition of *N*,*N*′-diisopropylethylamine. The reaction mixture was evaporated and dried under vacuum. The voluminous yellow solid was purified by column chromatography (silica gel, CH_2Cl_2/MeOH 100:0→98:2) to give **6** (5.18 g, 5.97 mmol, 100 %) as a yellow solid. ESIMS (CH_2Cl_2/MeOH 99:1): m/z: 867.9 $[M+H]^+$.

Preparation of 7: Compound **6** (5.00 g, 5.77 mmol) and activated iron powder (6.44 g, 115 mmol) were suspended in EtOH/H_2O 2:1 (300 mL). The reaction mixture was heated to 60 °C to solubilize **6**, and HCl (37 %) was slowly added until the reaction started to bubble (15 mL). The reaction mixture was then heated at reflux for 12 h. The excess iron powder was removed by decantation, washed with dichloromethane, and the organic solvents were evaporated. A solution of Na_4EDTA (60 g; EDTA = ethylenediaminetetraacetic acid) in H_2O (300 mL) and CH_2Cl_2 (500 mL) was added to the aqueous layer. A suspension was thus partitioned between a red aqueous phase (pH 8.0) and a yellow organic one. H_2O_2 (5 mL) was added and the pH was adjusted to 8.5 with an aqueous NH_4OH (25 %) solution. The biphasic solution was stirred for 30 min and the organic layer was separated from the dark-red aqueous phase, which was further extracted with CH_2Cl_2 (3 × 100 mL). The combined organic layers were dried over anhydrous $MgSO_4$, filtered, and evaporated to dryness. The white solid was purified by column chromatography (silica gel, CH_2Cl_2/MeOH 98:2) to yield **7** (3.50 g, 4.54 mmol, 79 %) as a white solid. When required, **7** can be crystallized from CH_3CN or by slow evaporation from a CH_2Cl_2/MeOH mixture. X-ray quality crystals can be obtained with the latter method. ^{1}H NMR (400 MHz, $CDCl_3$): $\delta = 1.32$ (t, $^3J = 7.1$ Hz, 6H), 4.31 (s, 2H), 5.03 (q, $^3J = 7.1$ Hz, 4H), 5.32 (s, 4H), 7.19 (dd, $^3J = 7.6$ Hz, $^4J = 1.3$ Hz, 2H), 7.26 (dd, $^3J = 8.4$ Hz, $^4J = 1.5$ Hz, 2H), 7.34–7.60 (m, 16H), 7.79 (s, 2H), 8.27 (d, $^3J = 8.5$ Hz, 2H), 8.6 ppm (d, $^3J = 8.5$ Hz, 2H); ^{13}C NMR (100 MHz, $CDCl_3$): $\delta = 15.20$, 41.11, 70.82, 109.47, 109.98, 119.66, 120.08, 122.03, 124.99, 127.34, 128.10, 128.18, 128.51, 128.89, 132.24, 136.16, 136.37, 136.82, 139.51, 143.08, 149.19, 149.49, 155.08 ppm; ESIMS (CH_2Cl_2/MeOH 99:1): m/z: 771.5 $[M+H]^+$, 1542.3 $[2M+H]^+$.

Preparation of L12b: The reaction was carried out under a nitrogen atmosphere. Compound **7** (1.50 g, 1.95 mmol) was dissolved in dry CH_2Cl_2 (50 mL). A BBr_3 solution in CH_2Cl_2 (1 M, 19.5 mL, 19.50 mmol) was added through a septum. The colorless solution quickly turned red and a beige precipitate formed, which was slowly transformed into a reddish oil. The reaction mixture was stirred for 12 h and methanol (30 mL) was slowly added to destroy the excess of BBr_3 (a strongly exothermic reaction). The reaction mixture was evaporated and dried under vacuum. The red solid was suspended in H_2O (100 mL) and sonicated for 5 min to obtain an homogeneous suspension. Aqueous saturated $NaHCO_3$ was slowly added (over about 1 h) to adjust the pH to 7.5. The colorless precipitate was filtered and washed with water to completely remove benzyl bromide. The solid was dried for 2 h under vacuum at 120 °C and yielded **L12b** (1.08 g, 1.83 mmol, 94 %) as a beige solid. ^{1}H NMR (400 MHz, [D$_6$]DMSO): $\delta = 1.40$ (t, $^3J = 7.1$ Hz, 6H), 4.25 (s, 2H), 5.07 (q, $^3J = 7.1$ Hz, 4H), 7.20 (dd, $^3J = 7.2$ Hz, $^4J = 1.6$ Hz, 2H), 7.31 (dd, $^3J = 8.5$ Hz, $^4J = 1.6$ Hz, 2H), 1.44–1.53 (m, 4H), 7.64 (d, $^3J = 8.5$ Hz, 2H), 7.70 (s, 2H), 8.41 (d, $^3J = 8.7$ Hz, 2H), 8.45 (d, $^3J = 8.7$ Hz, 2H), 9.83 ppm (s, 2H); ESIMS (DMSO): m/z: 591.5 $[M+H]^+$, 1182.3 $[2M+H]^+$; elemental analysis calcd (%) for $C_{37}H_{30}N_6O_2 \cdot 1.17\,H_2O$: C 72.63, H 5.33, N 13.74; found: C 72.67, H 5.04, N 13.41.

Preparation of the [Ln$_2$(L12b-2H)$_3$] (Ln = La, Nd, Eu, Y, and Lu) complexes: Ligand **L12b** (20 mg, 3.38×10^{-5} mol, 1 equiv) was suspended in CH_3CN (20 mL), shortly sonicated, and $Ln(OTf)_3 \cdot x\,H_2O$ (2.27×10^{-5} mol) was added. The solid rapidly disappeared and the color of the solution changed from colorless to yellow or pale orange after 5 min heating at 65 °C. An excess of solid K_2CO_3 (2 equiv per phenol function) was added and the solution was stirred at 65 °C for 12 h. During this time the solutions turned orange. The Ln = La, Nd, and Eu solutions are limpid after this treatment, whereas we observed the formation of an orange precipitate for the Ln = Y- and Lu-containing solutions. The reaction mixtures were precipitated with Et_2O (50 mL) and cooled (0 °C). The orange precipitates were filtered and washed with water to remove all the inorganic salts, then washed with Et_2O and dried under vacuum at 100 °C for 24 h to give binuclear complexes [Ln$_2$(**L12b**-2H)$_3$]·$x\,H_2O$ (Table S4 in the Supporting Information). The resulting solids varied from yellow [La$_2$(**L12b**-2H)$_3$] to dark red [Lu$_2$(**L12b**-2H)$_3$]. Suitable X-ray quality crystals of [Nd$_2$(**L12b**-2H)$_3$] were obtained by slow diffusion of Et_2O into a diluted solution of the complex in CH_3CN.

Preparation of [Ln$_2$(L12b-2H)$_3$] (Ln = La, Nd, Eu, and Y) samples for ^{1}H NMR spectroscopy in CD_3CN: Ligand **L12b** (5.0 mg, 8.46×10^{-6} mmol, 1 equiv) was suspended in CD_3CN (0.5 mL) and shortly sonicated. $Ln(OTf)_3 \cdot x\,H_2O$ (5.67×10^{-6} mmol, 0.67 equiv) was dissolved in CD_3CN (0.25 mL). The lanthanide solution was poured into the ligand solution. The volume of the reaction mixture was adjusted to 1 mL by addition of CD_3CN (0.25 mL). The mixture was heated at 65 °C for 30 min to get a yellow or pale orange solution. An excess of solid K_2CO_3 (about 2 equiv per phenol function) was added and the suspension was stirred at

65 °C for 1 h. Filtration through a membrane (0.25 μm porosity) directly in a 5 mm NMR spectroscopy tube allowed the subsequent recording of the ^{1}H NMR spectra. An orange precipitate formed upon waiting, a tendency that was more pronounced for small lanthanide ions.

Preparation of the samples for ^{1}H NMR spectroscopy and ESIMS titrations in [D$_6$]DMSO: $NBu_4OH{\cdot}30H_2O$ (0.5 mL, 1.00×10^{-2} M, 2 equiv) in [D$_6$]DMSO was added to a solution of **L12b** (5.00×10^{-3} M) in [D$_6$]DMSO. The solution immediately turned red and the ^{1}H NMR spectrum confirmed the quantitative formation of [**L12b**-2H](nBu$_4$N)$_2$. After a few minutes, the solution turned brown and side products precipitated. Consequently, aliquots of Ln(OTf)$_3{\cdot}x$H$_2$O (Ln = La, Nd, Eu, Y, and Lu; 0.67, 1.0, and 2.0 equiv) from stock solutions (3.35×10^{-3} M in [D$_6$]DMSO) were to be added immediately. The metal-stabilized solutions were then stirred at 65 °C for 1 h (precipitates disappeared after 5 min) before recording ^{1}H NMR spectra at 25 °C. The solutions were prepared under the same conditions for ESIMS titrations, except that 1) nondeuterated DMSO was used, and 2) the solutions were eventually diluted 10 times and 2% MeOH was added before recording the spectra.

Spectroscopic measurements: Spectrophotometric titrations were performed using a J&M diode array spectrometer (Tidas series) connected to an external computer. In a typical experiment, 50 mL of ligand in CH_2Cl_2/MeOH 1:1 (10^{-4} M) were titrated at 298 K with a solution of Ln(OTf)$_3{\cdot}x$H$_2$O (10^{-3} M) in CH_2Cl_2/MeOH 1:1 under an inert atmosphere. After each addition of 0.20 mL, the absorbance was recorded using Hellma optrodes (optical path length 0.1 cm) immersed in the titration vessel controlled by a thermostat and connected to the spectrometer. Mathematical treatment of the spectrophotometric titrations was performed using factor analysis[32] and with the SPECFIT program.[33] ^{1}H and ^{13}C NMR spectra were recorded at 298 K using a Bruker Avance 400 MHz spectrometer. Chemical shifts are given in ppm with respect to TMS. Pneumatically assisted electrospray mass spectra (ESIMS) were recorded from 10^{-4} M solutions using an Applied Biosystems API 150EX LC/MS system equipped with a Turbo Ionspray source. Least-square fits were performed using Microsoft Excel.[44] Elemental analyses were performed by Dr. H. Eder from the Microchemical Laboratory of the University of Geneva.

X-ray crystallography: Summary of crystal data, intensity measurements, and structure refinements for **7**, and A-[Nd$_2$(**L12b**-2H)$_3$]]$_2{\cdot}$[B-[Nd$_2$(**L12b**-2H)$_3$]]$\cdot8CH_3CN\cdot4H_2O$ (**10**) are collected in Table S17 in the Supporting Information. All crystals were mounted on quartz fibers with protection oil. Cell dimensions and intensities were measured at 150 K using a Stoe IPDS diffractometer with graphite-monochromated $Mo_{K\alpha}$ radiation (λ = 0.71073 Å). Data were corrected for Lorentz and polarization effects and for absorption. The structures were solved by direct methods (SIR97),[45] and all other calculation were performed using ShelX97 (**7**)[46] XTAL (**10**)[47] systems and ORTEP[48] programs. CCDC-739143 (**7**) contains the supplementary crystallographic data for this paper. These data can be obtained free of charge from The Cambridge Crystallographic Data Centre via www.ccdc.cam.ac.uk/data_request/cif. The cif file of **10** is given in the Supporting Information.

Comments on the crystal structure of 7: All non-hydrogen atoms (59) were refined with anisotropic atomic displacement parameters. The hydrogen atoms were observed and refined with U_{iso} = 0.06 Å^2, except for one methyl (H40 to H42) and those of one terminal phenyl group (H8 to H12), for which the atomic positions of the hydrogen atoms were calculated and fixed during the refinement. The phenyl C11–C16 atoms were slightly disordered, but attempts to split the carbon atoms for forming two phenyl rings with variable population parameters did not improve refinement nor convergence. The maximum residual electronic density was located close to this aromatic cycle.

Comments on the crystal structure of 10: More than two hundred crystallization attempts provided some extremely fragile red crystals, from which only data collections of limited qualities could be obtained (high-angle reflections with small intensities, despite long exposition periods of 10 min, and attempts to increase the imaging plate (IP)/crystal distance of 90 mm to improve resolution at the cost of limiting the angular domain of $2\theta_{max}$ = 45°). In the best data collection, two independent neutral binuclear triple-stranded helical complexes possessing opposite helicities A-[Nd$_2$(**L12b**-2H)$_3$] (multiplicity: 8) and B-[Nd$_2$(**L12b**-2H)$_3$] (multiplicity: 4) were found in the unit cell together with interstitial solvent molecules, thus leading to the complete chemical formula {A-[Nd$_2$(**L12b**-2H)$_3$]}$_2{\cdot}${B-[Nd$_2$(**L12b**-2H)$_3$]}$\cdot8CH_3CN\cdot4H_2O$ (**10**) with Z = 4. B-[Nd$_2$(**L12b**-2H)$_3$] was located on a crystallographic twofold axis passing through C19e. All hydrogen atoms were calculated and fixed (U_{iso} = 0.06 Å^2). All other atoms were refined with isotropic atomic displacement parameters, except the Nd atoms (anisotropic). The ethyl groups connected to the benzimidazole rings were disordered and gave large U_{iso} parameters, and so did the terminal hydroxyquinoline rings, which were thus refined with restraints on bond lengths and bond angles (235 restraints). The solvent molecules were refined with fixed U_{iso} and blocked during the refinement except for one acetonitrile molecule (N2sC3sC4s). According to the limited quality of this crystal structure, but considering its importance for confirming the formation of a triple-stranded helicate with intermetallic contact distance of 9.0 Å, we have not incorporated it into the CCDC file, but have instead provided the cif file in the Supporting Information.

Acknowledgements

We thank Johan Varin and Laetitia Gaillard for technical support. Financial support from the Swiss National Science Foundation is gratefully acknowledged.

[1] a) C. Piguet, G. Bernardinelli, A. F. Williams, *Angew. Chem.* **1992**, *102*, 1530–1532; *Angew. Chem. Int. Ed. Engl.* **1992**, *31*, 1622–1624; b) C. Piguet, J.-C. G. Bünzli, G. Bernardinelli, G. Hopfgartner, A. F. Williams, *J. Am. Chem. Soc.* **1993**, *115*, 8197–8296.

[2] a) N. Martin, J.-C. G. Bünzli, V. McKee, C. Piguet, G. Hopfgartner, *Inorg. Chem.* **1998**, *37*, 577–589; b) K. Zeckert, J. Hamacek, J.-P. Rivera, S. Floquet, A. Pinto, M. Borkovec, C. Piguet, *J. Am. Chem. Soc.* **2004**, *126*, 11589–11601.

[3] a) M. Elhabiri, R. Scopelliti, J.-C. G. Bünzli, C. Piguet, *J. Am. Chem. Soc.* **1999**, *121*, 10747–10762; b) M. Elhabiri, J. Hamacek, J.-C. G. Bünzli, A. M. Albrecht-Gary, *Eur. J. Inorg. Chem.* **2004**, 51–62.

[4] a) S. Floquet, N. Ouali, B. Bocquet, G. Bernardinelli, D. Imbert, J.-C. G. Bünzli, G. Hopfgartner, C. Piguet, *Chem. Eur. J.* **2003**, *9*, 1860–1875; b) S. Floquet, M. Borkovec, G. Bernardinelli, A. Pinto, L.-A. Leuthold, G. Hopfgartner, D. Imbert, J.-C. G. Bünzli, C. Piguet, *Chem. Eur. J.* **2004**, *10*, 1091–1105.

[5] a) K. Zeckert, J. Hamacek, J.-M. Senegas, N. Dalla-Favera, S. Floquet, G. Bernardinelli, C. Piguet, *Angew. Chem.* **2005**, *117*, 8168–8172; *Angew. Chem. Int. Ed.* **2005**, *44*, 7954–7958; b) N. Dalla-Favera, J. Hamacek, M. Borkovec, D. Jeannerat, F. Gumy, J.-C. G. Bünzli, G. Ercolani, C. Piguet, *Chem. Eur. J.* **2008**, *14*, 2994–3005.

[6] J. L. Lessmann, W. de W. Horrocks, Jr., *Inorg. Chem.* **2000**, *39*, 3114–3124.

[7] a) C. D. B. Vandevyver, A.-S. Chauvin, S. Comby, J.-C. G. Bünzli, *Chem. Commun.* **2007**, 1716–1718; b) A.-S. Chauvin, S. Comby, B. Song, C. D. B. Vandevyver, F. Thomas, J.-C. G. Bünzli, *Chem. Eur. J.* **2007**, *13*, 9515–9526; c) A.-S. Chauvin, S. Comby, B. Song, C. D. B. Vandevyver, J.-C. G. Bünzli, *Chem. Eur. J.* **2008**, *14*, 1726–1739; d) E. Deiters, B. Song, A.-S. Chauvin, C. D. B. Vandevyver, J.-C. G. Bünzli, *New J. Chem.* **2008**, *32*, 1140–1152; e) J.-C. G. Bünzli, A.-S. Chauvin, C. D. B. Vandevyver, S. Bo, S. Comby, *Ann. N. Y. Acad. Sci.* **2008**, *1130*, 97–105; f) B. Song, C. D. B. Vandevyver, A.-S. Chauvin, J.-C. G. Bünzli, *Org. Biomol. Chem.* **2008**, *6*, 4125–4133; g) B. Song, C. D. B. Vandevyver, E. Deiters, A.-S. Chauvin, I. Hemmilä, J.-C. G. Bünzli, *Analyst* **2008**, *133*, 1749–1756; h) J.-C. G. Bünzli, *Chem. Lett.* **2009**, *38*, 104–109; i) E. Deiters, B. Song, A.-S. Chauvin, C. D. B. Vandevyver, F. Gumy, J.-C. G. Bünzli, *Chem. Eur. J.* **2009**, *15*, 885–900.

[8] a) A. Dossing, *Eur. J. Inorg. Chem.* **2005**, 1425–1434; b) S. Comby, J.-C. G. Bünzli in *Handbook on the Physics and Chemistry of Rare Earths, Vol. 37* (Eds.: K. A. Gschneidner, Jr., J.-C. G. Bünzli, V. K.

Pecharsky), Elsevier, Amsterdam, **2007**, pp. 217–470; c) T. Nishioka, K. Fukui, K. Matsumoto in *Handbook on the Physics and Chemistry of Rare Earths, Vol. 37* (Eds.: K. A. Gschneidner, Jr., J.-C. G. Bünzli, V. K. Pecharsky), Elsevier, Amsterdam, **2007**, pp. 171–220; d) M. D. Ward, *Coord. Chem. Rev.* **2007**, *251*, 1663–1677.

[9] A. Nonat, D. Imbert, J. Pécaut, M. Giraud, M. Mazzanti, *Inorg. Chem.* **2009**, *48*, 4207–4218.

[10] a) D. Imbert, S. Comby, A.-S. Chauvin, J.-C. G. Bünzli, *Chem. Commun.* **2005**, 1432–1434; b) M. Albrecht, O. Osetska, J. Klankermayer, R. Fröhlich, F. Gumy, J.-C. G. Bünzli, *Chem. Commun.* **2007**, 1834–1836; c) M. Albrecht, M. Fiege, O. Osetska, *Coord. Chem. Rev.* **2008**, *252*, 812–824.

[11] M. Albrecht, O. Osetska, R. Fröhlich, *Dalton Trans.* **2005**, 3757–3762.

[12] N. M. Shavaleev, R. Scopelliti, F. Gumy, J.-C. G. Bünzli, *Inorg. Chem.* **2008**, *47*, 9055–9068.

[13] M. Albrecht, O. Osetska, R. Fröhlich, J.-C. G. Bünzli, A. Aebischer, F. Gumy, J. Hamacek, *J. Am. Chem. Soc.* **2007**, *129*, 14178–14179.

[14] G. Ercolani, C. Piguet, M. Borkovec, J. Hamacek, *J. Phys. Chem. B* **2007**, *111*, 12195–12203.

[15] J. Hamacek, M. Borkovec, C. Piguet, *Dalton Trans.* **2006**, 1473–1490, and references therein.

[16] a) R. J. Motekaitis, A. E. Martell, R. A. Hancock, *Coord. Chem. Rev.* **1994**, *133*, 39–65; b) P. Caravan, T. Hedlund, S. Liu, S. Sjöberg, C. Orvig, *J. Am. Chem. Soc.* **1995**, *117*, 11230–11238; c) J.-M. Senegas, G. Bernardinelli, D. Imbert, J.-C. G. Bünzli, P.-Y. Morgantini, J. Weber, C. Piguet, *Inorg. Chem.* **2003**, *42*, 4680–4695.

[17] N. Dalla-Favera, J. Hamacek, M. Borkovec, D. Jeannerat, F. Gumy, J.-C. G. Bünzli, G. Ercolani, C. Piguet, *Chem. Eur. J.* **2008**, *14*, 2994–3005.

[18] G. Canard, C. Piguet, *Inorg. Chem.* **2007**, *46*, 3511–3522.

[19] T. Riis-Johannessen, N. Dalla Favera, T. Todorova, S. M. Huber, L. Gagliardi, C. Piguet, *Chem. Eur. J.* **2009**, DOI: 10.1002/chem.200900904.

[20] C. Caris, P. Baret, J.-L. Pierre, G. Serratrice, *Tetrahedron* **1996**, *52*, 4659–4672.

[21] C. Piguet, G. Bernardinelli, B. Bocquet, A. Quattropani, A. F. Williams, *J. Am. Chem. Soc.* **1992**, *114*, 7440–7491.

[22] C. Piguet, B. Bocquet, G. Hopfgartner, *Helv. Chim. Acta* **1994**, *77*, 931–942.

[23] F. H. Allen, O. Kennard, D. G. Watson, L. Brammer, O. A. G. R. Taylor, *J. Chem. Soc. Perkin Trans. 2* **1987**, S1–S19.

[24] J. H. Brewster, *Top. Curr. Chem.* **1974**, *46*, 29–71.

[25] N. Dalla Favera, L. Guénée, G. Bernardinelli, C. Piguet, *Dalton Trans.* **2009**, DOI: 10.1039/b905131g.

[26] R. D. Shannon, *Acta. Crystallogr. Sect. A* **1976**, *32*, 751–767. The ionic radii are calculated by using $r(N)=1.46$ Å and $r(O)=1.35$ Å and amount to $R_{Nd1}^{CN=9}=1.17$ Å, $R_{Nd2}^{CN=9}=1.19$ Å and $R_{Nd3}^{CN=9}=1.16$ Å in **10**, and $R_{Nd}^{CN=9}=1.17$ Å in *HHT*-[Nd(**L10**-2H)$_3$].

[27] a) I. D. Brown, D. Altermatt, *Acta Crystallogr. Sect. B* **1985**, *41*, 244–247; b) N. E. Brese, M. O'Keeffe, *Acta Crystallogr. Sect. B* **1991**, *47*, 192–197; c) I. D. Brown, *Acta Crystallogr. Sect. B* **1992**, *48*, 553–572; d) I. D. Brown, *The Chemical Bond in Inorganic Chemistry*, Oxford University Press, Oxford, **2002**.

[28] a) A. Trzesowska, R. Kruszynski, T. J. Bartczak, *Acta Crystallogr. Sect. B* **2004**, *60*, 174–178; b) A. Trzesowska, R. Kruszynski, T. J. Bartczak, *Acta Crystallogr. Sect. B* **2005**, *61*, 429–434; c) F. Zocchi, *J. Mol. Struct.* **2007**, *825–846*, 73–78.

[29] A. Escande, L. Guénée, K.-L. Buchwalder, C. Piguet, *Inorg. Chem.* **2009**, *48*, 1132–1147.

[30] I. D. Brown, *Acta Crystallogr. Sect. B* **1977**, *33*, 1305–1310.

[31] a) E. Leize, A. Jaffrezic, A. van Dorsselaer, *J. Mass Spectrom.* **1996**, *31*, 537–544; b) G. Hopfgartner, F. Vilbois, C. Piguet, *Rapid Commun. Mass Spectrom.* **1999**, *13*, 302–306.

[32] E. R. Malinowski, D. G. Howery, *Factor Analysis in Chemistry*, Wiley, New York, **1980**.

[33] a) H. Gampp, M. Maeder, C. J. Meyer, A. Zuberbühler, *Talanta* **1985**, *32*, 1133–1139; b) H. Gampp, M. Maeder, C. J. Meyer, A. Zuberbühler, *Talanta* **1986**, *33*, 943–951.

[34] a) C. Piguet, G. Bernardinelli, G. Hopfgartner, *Chem. Rev.* **1997**, *97*, 2005–2062; b) M. Albrecht, *Chem. Rev.* **2001**, *101*, 3457–3497.

[35] The diastereotopic methylene protons of the ethyl residues (H10 in Figure 5) provide two pseudo-sextets (ABX_3 spin system with $J^2 \approx 2J^3$) without implying any blocked rotations as suggested in ref. [12].

[36] K. Binnemans, K. Lodewyckx, T. Cardinaels, T. N. Parac-Vogt, C. Bourgogne, D. Guillon, B. Donnio, *Eur. J. Inorg. Chem.* **2006**, 150–157.

[37] a) S. W. Benson, *J. Am. Chem. Soc.* **1958**, *80*, 5151–5154; b) S. W. Benson, *Thermochemical Kinetics*, 2nd ed., Wiley-Interscience, New York, **1976**, pp. 37–39.

[38] M. R. Willcott, R. E. Lenkinski, R. E. Davis, *J. Am. Chem. Soc.* **1972**, *94*, 1742–1744,
$AF_{Ln}\sqrt{[\sum_i (\log\beta_{i,exp}^{Ln,L}-\log\beta_{i,calcd}^{Ln,L})^2]/[\sum_i (\log\beta_{i,exp}^{Ln,L})^2]}$.

[39] A. Mulder, J. Huskens, D. N. Reinhoudt, *Org. Biomol. Chem.* **2004**, *2*, 3409–3424. The effective concentration (c^{eff}) is often referred to as the effective molarity (EM) when focusing on its experimental value. For the sake of clarity, we will only use in this work the effective concentration for both the concept and its experimental value.

[40] C. Marchal, Y. Filinchuk, X.-Y. Chen, D. Imbert, M. Mazzanti, *Chem. Eur. J.* **2009**, *15*, 5273–5288.

[41] N. Kerbellec, D. Kustaryono, V. Haquin, M. Etienne, C. Daiguebonne, O. Guillou, *Inorg. Chem.* **2009**, *48*, 2837–2843.

[42] J. F. Desreux in *Lanthanide Probes in Life, Chemical and Earth Sciences* (Eds.: J.-C. G. Bünzli, G. R. Choppin), Elsevier, Amsterdam, **1989**, Chapter 2, p. 43.

[43] G. Schwarzenbach, *Complexometric Titrations*, Chapman & Hall, London, **1957**, p. 8.

[44] Microsoft Excel 2003, Microsoft Corporation, USA.

[45] A. Altomare, M. C. Burla, M. Camalli, G. Cascarano, C. Giacovazzo, A. Guagliardi, G. Moliterni, G. Polidori and R. Spagna, *J. Appl. Crystallogr.* **1999**, *32*, 115–119.

[46] SHELXL97, Program for the Solution and Refinement of Crystal Structures, G. M. Sheldrick, University of Göttingen, Göttingen, **1997**.

[47] XTAL 3.2, User's Manual (Eds.: S. R. Hall, H. D. Flack, J. M. Stewart), Universities of Western Australia and Maryland, **1989**.

[48] ORTEP II; Report ORNL-5138, C. K. Johnson, Oak Ridge National Laboratory: Oak Ridge, **1976**.

Received: July 21, 2009
Published online: September 25, 2009

